G protein-coupled receptor-mediated calcium signaling in astrocytes

Maurizio de Pittà, Eshel Ben-Jacob, Hugues Berry

G protein-coupled receptor-mediated calcium signaling in astrocytes

Maurizio De Pittà
EPI BEAGLE, INRIA Rhône-Alpes, Villeurbanne, France

Eshel Ben-Jacob[†]
School of Physics and Astronomy, Tel Aviv University, Ramat Aviv, Israel

Hugues Berry
EPI BEAGLE, INRIA Rhône-Alpes, Villeurbanne, France

February 12, 2018

Abstract

Astrocytes express a large variety of G protein-coupled receptors (GPCRs) which mediate the transduction of extracellular signals into intracellular calcium responses. This transduction is provided by a complex network of biochemical reactions which mobilizes a wealth of possible calcium-mobilizing second messenger molecules. Inositol 1,4,5-trisphosphate is probably the best known of these molecules whose enzymes for its production and degradation are nonetheless calcium-dependent. We present a biophysical modeling approach based on the assumption of Michaelis-Menten enzyme kinetics, to effectively describe GPCR-mediated astrocytic calcium signals. Our model is then used to study different mechanisms at play in stimulus encoding by shape and frequency of calcium oscillations in astrocytes.

1 Introduction

Calcium signaling is the most common measured readout of astrocyte activity in response to stimulation, be it by synaptic activity, by neuromodulators diffusing in the extracellular milieu, or by exogenous chemical, mechanical or optical stimuli. In this perspective, the individual astrocytic Ca^{2+} transient is thought, to some extent, as an integration of the triggering stimulus (Perea and Araque, 005a), and is thus regarded as an encoding or decoding of this stimulus, depending on the point of view (Carmignoto, 2000; De Pittà et al., 2013).

Multiple and varied are the spatiotemporal patterns of Ca^{2+} elevations recorded from astrocytes in response to stimulation, each possibly carrying its own encoding (Bindocci et al., 2017). Insofar as different encoding modes could correspond to different downstream signaling, including gliotransmission and thereby regulation of synaptic function, understanding the biophysical mechanisms underlying rich Ca^{2+} dynamics in astrocytes is crucial.

Calcium-induced Ca^{2+} release (CICR) from the endoplasmic reticulum (ER) is arguably the best characterized mechanism of Ca^{2+} signaling in astrocytes (Zorec et al., 2012). It ensues from nonlinear properties of Ca^{2+} channels which are found on the ER membrane and are gated by the combined action of cytosolic Ca^{2+} and the second messenger molecule inositol 1,4,5-trisphosphate (IP_3) (Shinohara et al., 2011, see also Chapters 2–4). This second messenger

[†]Deceased June 5, 2015.

molecule can be produced by the astrocyte either spontaneously or, notably, in response to activation by extracellular insults activation of G protein-coupled receptors (GPCRs) found on the cell's plasma membrane (Parri and Crunelli, 2003; Panatier et al., 2011; Volterra et al., 2014). Hence, IP_3 together with these receptors, can be regarded as integral components of the interface whereby an astrocyte transduces extracellular insults into Ca^{2+} responses (Marinissen and Gutkind, 2001). Characterizing this interface is thus an essential step in our understanding of the emerging complexity of Ca^{2+} signals, and we devote this chapter to this purpose. In the first part of the chapter, we will present a concise framework to model intracellular IP_3 signaling in astrocytes. This framework is general and can easily be extended to include additional biological details, such as for example, the regulation of GPCR binding efficiency by protein kinase C. Some of the models presented in this chapter are also subjected to revision and comparison with other astrocyte models in Chapters 16 and 18.

2 Modeling intracellular IP_3 dynamics

2.1 Agonist-mediated IP_3 production

G protein-coupled receptors form a large family of receptors which owe their name to their extensively studied interaction with heterotrimeric G proteins (composed of an α, β and γ subunit) which undergo conformational changes that lead to the exchange of GDP for GTP, bound to the α-subunit, following receptor activation. Consequently, the Gα- and G$\beta\gamma$-subunits stimulate enzymes thereby activating or inhibiting the production of a variety of second messengers (Marinissen and Gutkind, 2001).

Among all GPCRs, those that contain the $G\alpha_q$ subunit are linked with the cascade of chemical reactions that leads to IP_3 synthesis. There, the $G\alpha_q$ subunit promotes activation of the enzyme pospholipase Cβ (PLCβ) which hydrolizes the plasma membrane lipid phosphatidylinositol 4,5-bisphosphate (PIP_2) into diacylglycerol (DAG) and IP_3 (Rebecchi and Pentyala, 2000). Examples of such receptors expressed by astrocytes ex vivo and in vivo are the type I metabotropic glutamate receptor 1 and 5 (mGluR1/5) (Wang et al., 2006; Sun et al., 2013), the purinergic receptor P_2Y_1 (Jourdain et al., 2007; Di Castro et al., 2011; Sun et al., 2013), the muscarinic receptor mAchR1α (Takata et al., 2011; Chen et al., 2012; Navarrete et al., 2012) and the adrenergic α_1 receptor (Bekar et al., 2008; Ding et al., 2013). While these receptors bind different agonists, and likely display receptor-specific binding kinetics, they all share the same downstream signaling pathway and therefore may be modeled in a similar fashion.

Several are the available models for $G\alpha_q$-containing receptors, and the choice of what model to use rather than another depends on the level of biological detail and the questions one is interested in. Here our focus is on the rate of IP_3 production upon activation of these receptors, so we wish to keep as simple as possible the description of the reactions that regulate the activation of PLCβ by α_q, β and γ subunits. This is possible, assuming that these reactions are much faster than the downstream ones that result in IP_3 production. In this case, a *quasi steady-state approximation* (QSSA) holds whereby, in the series of reactions that leads from receptor agonist binding to activation of PLCβ, the intermediate reactions involving the three receptor's subunits are at equilibrium on the time scale of the production of activated PLCβ. Accordingly, assuming that on average the receptor at rest (R) requires n molecules of an agonist (A) to promote activation of PLCβ (R^*) at rate O_N, we can write

$$\mathrm{R} + n\,\mathrm{A} \xrightarrow{O_N} \mathrm{R}^* \tag{1}$$

We further make another assumption: that the cascade of reactions that leads to GPCR-mediated IP_3 synthesis has a Michaelis-Menten kinetics (see Appendix A.2), so the IP_3 pro-

duction by PLCβ (J_β) can be taken proportional to the fraction of bound receptors, defined as $\Gamma_A = [\mathrm{R}^*]/[\mathrm{R}]_\mathrm{T}$, with $[\mathrm{R}]_\mathrm{T}$=$[\mathrm{R}] + [\mathrm{R}^*]$ being the total receptor concentration at the site of IP_3 production, i.e.,

$$J_\beta = O_\beta \cdot \Gamma_A \tag{2}$$

In the above equation O_β is the maximal rate of IP_3 production by PLCβ and lumps information on receptor surface density as well as on the size of the PIP_2 reservoir. Importantly, these two quantities may not be fixed, insofar as receptors are subjected to desensitization, internalization and recycling, and the reservoir of PIP_2 could also be modulated by cytosolic Ca^{2+} and IP_3 (Rhee and Bae, 1997). The reader interested in modeling these aspects may refer to Lemon et al. (2003). In the following, we will assume O_β constant for simplicity.

To seek an expression for J_β, termination of PLCβ signaling has to be considered. With this regard, as illustrated in Figure 1A, there are two possible pathways whereby IP_3 production by PLCβ ends (Rebecchi and Pentyala, 2000). One is by reconstitution of the inactive G protein heterotrimer, and coincides with unbinding of the agonist from the receptor, due to the intrinsic GTPase activity of the activated $G\alpha_q$ subunit. The other is by phosphorylation of the receptor, the $G\alpha_q$ subunit, PLCβ or some combination thereof by conventional protein kinases C (cPKC) (Ryu et al., 1990; Codazzi et al., 2001). This phosphorylation modulates either receptor affinity for agonist binding, or coupling of the bound receptor with the G protein, or coupling of the activated G protein with PLCβ, ultimately resulting in receptor desensitization (Fisher, 1995).

Denoting by cPKC* the active, receptor-phosphorylating kinase C, termination of PLCβ-mediated IP_3 production can then be modeled by the following pair of chemical reactions:

$$\mathrm{R}^* \xrightarrow{\Omega_N} \mathrm{R} + n\,\mathrm{A} \tag{3}$$

$$\mathrm{cPKC}^* + \mathrm{R}^* \underset{\Omega_{KR}}{\overset{O_{KR}}{\rightleftharpoons}} \mathrm{cPKC}^*\!-\!\mathrm{R}^* \xrightarrow{\Omega_K} \mathrm{cPKC}^* + \mathrm{R} + n\,\mathrm{A} \tag{4}$$

From equations 3–4 we have:

$$\frac{\mathrm{d}\mathrm{R}^*}{\mathrm{d}t} = O_N[\mathrm{A}]^n[\mathrm{R}] - \Omega_N[\mathrm{R}^*] - O_{KR}[\mathrm{cPKC}^*][\mathrm{R}^*] + \Omega_{KR}[\mathrm{cPKC}^*\!-\!\mathrm{R}^*] \tag{5}$$

$$\frac{\mathrm{d}[\mathrm{cPKC}^*\!-\!\mathrm{R}^*]}{\mathrm{d}t} = O_{KR}[\mathrm{cPKC}^*][\mathrm{R}^*] - (\Omega_{KR} + \Omega_K)[\mathrm{cPKC}^*\!-\!\mathrm{R}^*] \tag{6}$$

Assuming that production of the intermediate kinase-receptor complex is at quasi steady state in reaction 4, i.e. $\mathrm{d}[\mathrm{cPKC}^*\!-\!\mathrm{R}^*]/\mathrm{d}t \approx 0$, provides (equation **??**)

$$[\mathrm{cPKC}^*\!-\!\mathrm{R}^*] = \frac{O_{KR}}{\Omega_{KR} + \Omega_K}[\mathrm{cPKC}^*][\mathrm{R}^*] \tag{7}$$

Then, substituting this latter equation in equation 5 gives

$$\begin{aligned}\frac{\mathrm{d}\mathrm{R}^*}{\mathrm{d}t} &= O_N[\mathrm{A}]^n[\mathrm{R}] - \Omega_N[\mathrm{R}^*] - O_{KR}\left(1 - \frac{\Omega_{KR}}{\Omega_{KR} + \Omega_K}\right)[\mathrm{cPKC}^*][\mathrm{R}^*] \\ &= O_N[\mathrm{A}]^n[\mathrm{R}] - \Omega_N[\mathrm{R}^*] - O_K[\mathrm{cPKC}^*][\mathrm{R}^*]\end{aligned} \tag{8}$$

where we defined $O_K = O_{KR}\,(1 - \Omega_{KR}/\,(\Omega_{KR} + \Omega_K))$.

To retrieve an equation for [cPKC*], we consider the fact that activation of cPKC requires binding to the kinase of free cytosolic Ca^{2+} (C) and DAG, but only if Ca^{2+} binds first, cPKC can get sensibly activated by DAG (Oancea and Meyer, 1998). Accordingly, the following sequential binding reaction scheme for cPKC activation may be assumed:

$$\mathrm{cPKC} + \mathrm{Ca}^{2+} \underset{\Omega_{KC}}{\overset{O_{KC}}{\rightleftharpoons}} \mathrm{cPKC}' \tag{9}$$

$$\mathrm{cPKC}' + \mathrm{DAG} \underset{\Omega_{KD}}{\overset{O_{KD}}{\rightleftharpoons}} \mathrm{cPKC}^* \tag{10}$$

where cPKC is the inactive kinase, and cPKC$'$ denotes the Ca^{2+}-bound kinase complex. By QSSA in reaction 4 it follows that the available activated kinase approximately equals to $[\mathrm{cPKC}^*]_\mathrm{T} = [\mathrm{cPKC}^*] + [\mathrm{cPKC}^* – \mathrm{R}^*] \approx [\mathrm{cPKC}^*]$. Moreover, it can be assumed that only a small fraction of cPKC$'$ is bound by DAG so that $[\mathrm{cPKC}^*] \ll [\mathrm{cPKC}']$. In this fashion, the available cPKC, denoted by $[\mathrm{cPKC}]_\mathrm{T}$, can be approximated by $[\mathrm{PKC}]_\mathrm{T} \approx [\mathrm{PKC}] + [\mathrm{PKC}']$. Accordingly, solving reactions 9 and 10 for $[\mathrm{PKC}^*]$ provides

$$\begin{aligned}
[\mathrm{cPKC}^*] &= \left([\mathrm{cPKC}^*] + [\mathrm{cPKC}']\right) \cdot \mathcal{H}_1\left([\mathrm{DAG}], K_{KD}\right) \\
&\approx [\mathrm{cPKC}'] \cdot \mathcal{H}_1\left([\mathrm{DAG}], K_{KD}\right) \\
&= [\mathrm{cPKC}]_\mathrm{T} \cdot \mathcal{H}_1\left(C, K_{KC}\right) \cdot \mathcal{H}_1\left([\mathrm{DAG}], K_{KD}\right)
\end{aligned} \tag{11}$$

where $K_{KD} = \Omega_{KD}/O_{KD}$ and $K_{KC} = \Omega_{KC}/O_{KC}$, and $\mathcal{H}_1(x, K)$ denotes the Hill function $x/(x+K)$ (Appendix A.1). In practice the activation of the kinase consists of two sequential translocations to the plasma membrane of its C2 and $C1_2$ domains (Oancea and Meyer, 1998). The translocation of C2 is regulated by Ca^{2+} whereas that of $C1_2$ is by DAG. In this process however, experiments showed that the initial translocation of C2 is the rate limiting step for kinase activation (Shinomura et al., 1991), inasmuch as $C1_2$ translocation rapidly follows that of C2 (Codazzi et al., 2001). This agrees with the notion that the cPKC affinity for DAG is regarded to be much higher than the affinity of the kinase for Ca^{2+}, i.e. $K_{KD} \ll K_{KC}$ (Nishizuka, 1995). Since the product of two Hill functions with widely separated constants can be approximated by the Hill function with the largest constant (De Pittà et al., 2009), equation 11 can be rewritten as

$$[\mathrm{cPKC}^*] \approx [\mathrm{cPKC}]_\mathrm{T} \cdot \mathcal{H}_1\left(C, K_{KC}\right) \tag{12}$$

which, once replaced in equation 8, gives:

$$\frac{\mathrm{d}[\mathrm{R}^*]}{\mathrm{d}t} = O_N[\mathrm{A}]^n[\mathrm{R}] - \Omega_N\left(1 + \frac{O_K[\mathrm{cPKC}]_\mathrm{T}}{\Omega_N}\,\mathcal{H}_1\left(C, K_{KC}\right)\right)[\mathrm{R}^*] \tag{13}$$

Finally, dividing both left and right terms in the above equation by $[\mathrm{R}]_\mathrm{T}$, equation 13 can be rewritten as

$$\frac{\mathrm{d}\Gamma_A}{\mathrm{d}t} = O_N[\mathrm{A}]^n\,(1-\Gamma_A) - \Omega_N\left(1 + \zeta \cdot \mathcal{H}_1\left(C, K_{KC}\right)\right)\Gamma_A \tag{14}$$

where $\zeta = O_{KC}[\mathrm{cPKC}]_\mathrm{T}/\Omega_N$ quantifies the maximal receptor desensitization by cPKC. In the approximation that receptor binding and activation is much faster than the effective PLCβ-mediated IP_3 production, Γ_A can be solved for the steady state. In this fashion, IP_3 production by PLCβ in equation 2 becomes

$$J_\beta = O_\beta \cdot \mathcal{H}_n\left([\mathrm{A}], \left(K_N\left(1 + \zeta\,\mathcal{H}_1\left(C, K_{KC}\right)\right)\right)^{\frac{1}{n}}\right) \tag{15}$$

where $K_N = \Omega_N/O_N$. The Hill coefficient n denotes cooperativity of the binding reaction of the agonist with the receptor and is both receptor and agonist specific. For example, glutamate binding to subtype 1 mGluRs, such as those expressed by astrocytes (Gallo and Ghiani, 2000), is characterized by negative cooperativity and found in association with a Hill coefficient of $n = 0.48 – 0.88$ (Suzuki et al., 2004). On the contrary, binding of ATP to P_2Y_1Rs of dorsal spinal cord astrocytes from rats is characterized instead by almost no cooperativity and $n = 0.9 – 1$ (Fam et al., 2000).

2.2 IP_3 production by receptors with α subunits other than q-type

A series of other astrocytic GPCRs, that traditionally associate with non-α_q subunits, have also been reported to mediate IP_3-triggered CICR, both in situ and in vivo. These include $G\alpha_{i/o}$-coupled $GABA_B$ receptors (Kang et al., 1998; Serrano et al., 2006; Mariotti et al., 2016), endocannabinoid CB_1 receptors (Navarrete and Araque, 2008; Min and Nevian, 2012), adenosinergic A_1 receptors (Cristóvão-Ferreira et al., 2013), adrenergic α_2 receptors (Bekar et al., 2008), and dopaminergic $D_{2/3}$ receptors (Jennings et al., 2017); as well as $G\alpha_s$-coupled receptors like adenosine A_{2A} receptors (Cristóvão-Ferreira et al., 2013), and dopamine $D_{1/5}$ receptors (Jennings et al., 2017). $\alpha_{i/o}$ and α_s subunits are not expected to be linked with IP_3 synthesis (Marinissen and Gutkind, 2001), rather they respectively inhibit or stimulate intracellular production of cAMP. Therefore the mechanism whereby these receptors could also promote mobilization of Ca^{2+} from IP_3-sensitive ER stores remains a matter of investigation.

One obvious possibility is that some of these receptors could be atypical in astrocytes and also be coupled with $G\alpha_q$, as it seems the case for example of astrocytic CB_1Rs in the hippocampus (Navarrete and Araque, 2008) and in the basal ganglia (Martín et al., 2015). Biased agonism could also be another possibility since the spatiotemporal pattern of agonist action on GPCRs could be quite different depending on agonist-binding kinetics of the receptor, especially if agonists differentially engage dynamic signalling and regulatory processes (Overington et al., 2006), such as in the likely scenario of synapse-astrocyte interactions (Heller and Rusakov, 2015). However, there is not yet direct structural evidence for distinct receptor conformations linked to specific signals such as distinct G protein classes, and future studies are required to compare crystal structures of astrocytic GPCRs bound to biased and unbiased ligands to establish these relationships (Violin et al., 2014).

Alternatively, other signaling pathways mediated by cAMP that result in CICR could also be envisaged. In particular, Doengi et al. (2009) reported that GABA-evoked astrocytic Ca^{2+} events in the olfactory bulb are fully prevented by blockers of astrocytic GABA transporters (GATs), but only partially by $GABA_B$ antagonists. GAT activation leads to an increase of intracellular Na^+, since this ion is cotransported with GABA, and such increase indirectly inhibits the Na^+/Ca^{2+} exchanger on the plasma membrane. In turn, the ensuing Ca^{2+} increase could be sufficient to induce Ca^{2+} release from internal stores by stimulation of endogenous IP_3 production (Losi et al., 2014, see the following Section). This possibility is further corroborated by the observation that astrocytic GATs could indeed be inhibited or stimulated respectively by A_1Rs or A_{2A}Rs (Cristóvão-Ferreira et al., 2013).

Yet other mechanisms could be at play for different receptors. Dopaminergic receptors for example could either increase ($D_{1/5}$ receptors) or decrease ($D_{2/3}$ receptors) intracellular Ca^{2+} levels in astrocytes (Jennings et al., 2017). This could indeed be explained assuming a possible action of these receptors on GATs which, similarly to adenosinergic receptors, could respectively increase or reduce $GABA/Na^+$ cotransport into the cell, ultimately promoting or inhibiting CICR according to what was suggested for $GABA_B$Rs. However there is also evidence that nontoxic levels of dopamine could be metabolized by monoamine-oxidase in cultured astrocytes, resulting in the production of hydrogen peroxide (Vaarmann et al., 2010). This reactive oxygen species ultimately activates lipid peroxidation in the neighboring membranes which in turn triggers PLC-mediated IP_3 production and CICR. Overall these different scenarios unravel additional complexity in the possible mechanisms of GPCR-mediated CICR in astrocytes and call for future modeling efforts that are beyond the scope of this chapter.

2.3 Endogenous IP_3 production

Phospholipase Cδ (PLCδ) is the enzyme responsible of endogenous IP_3 production in astrocytes, that is IP_3 production that does not require external (i.e. exogenous) stimulation (Ochocka and Pawelczyk, 2003; Suh et al., 2008). The specific catalytic activity of this enzyme in the presence of cytosolic Ca^{2+} is 50- to 100-fold greater than Ca^{2+}-stimulated activity of PLCβ in the absence of activating G protein subunits (Rebecchi and Pentyala, 2000), suggesting that PLCδ is prominently activated by increases of intracellular Ca^{2+} (Rhee and Bae, 1997).

Figure 1B exemplifies the biochemical network associated with PLCδ activation. Structural and mutational studies of PLCδ complexes with Ca^{2+} and IP_3, revealed complex interactions of Ca^{2+} with several negatively charged residues within the PLCδ catalytic domain (Essen et al., 1996, 1997; Rhee and Bae, 1997), hinting cooperative binding of at least two Ca^{2+} ions with this enzyme (Essen et al., 1997). In agreement with these experimental findings, we model PLCδ-mediated IP_3 production (J_δ) as (Pawelczyk and Matecki, 1997; Höfer et al., 2002):

$$J_\delta = \hat{J}_\delta(I) \cdot \mathcal{H}_2\left(C, K_\delta\right) \tag{16}$$

where $\mathcal{H}_2\left(C, K_\delta\right)$ denotes the Hill function of C with coefficient 2 and affinity K_δ (Appendix B), and $\hat{J}_\delta(I)$ is the maximal rate of IP_3 production by PLCδ which depends on intracellular IP_3 (I). Experiments revealed that high IP_3 concentrations, i.e. $> 1\,\mu M$, inhibit PLCδ activity by competing with PIP_2 binding to the enzyme (Allen and Barres, 2009). Accordingly, the maximal PLCδdependent IP_3 production rate can be modeled by

$$\hat{J}_\delta(I) = \frac{O_\delta}{1 + \frac{I}{\kappa_\delta}} = O_\delta\left(1 - \mathcal{H}_1\left(I, \kappa_\delta\right)\right) \tag{17}$$

where O_δ is the maximal rate of IP_3 production by PLCδ and κ_δ is the inhibition constant of PLCδ activity.

2.4 IP_3 degradation

There are two pathways for IP_3 degradation in astrocytes. The first one is by dephosphorylation of IP_3 by inositol polyphosphate 5-phosphatase (IP-5P). The other one occurs through phosphorylation of IP_3 by the IP_3 3-kinase ($IP_3$3K). Both pathways could be Ca^{2+} dependent but in opposite ways: while the activity of $IP_3$3K is stimulated by cytosolic Ca^{2+} (Communi et al., 1997), IP-5P is inhibited instead (Communi et al., 2001) (Figure 2A). Thus, depending on the Ca^{2+} concentration in the cytoplasm, different mechanisms of IP_3 degradation could exist (Sims and Allbritton, 1998). Moreover, IP-5P-mediated IP_3 degradation could also be inhibited by competitive binding of inositol 1,3,4,5-tetrakisphosphate (IP_4) produced by IP_3-3K-mediated IP_3 phosphorylation (Connolly et al., 1987; Erneux et al., 1998), thereby making the two degradation pathways interdependent (Hermosura et al., 2000). However, we will not consider this aspect any further, since modeling of this reaction pathway requires a detailed consideration of the complex metabolic network underpinning degradation of the large family of inositol phosphates (Communi et al., 2001; Irvine and Schell, 2001). The reader interested in these aspects may refer to Dupont and Erneux (1997) for a sample modeling approach to the problem.

Both IP-5P-mediated dephosphorylation (J_{5P}) and $IP_3$3K-mediated phosphorylation of IP_3 (J_{3K}) can be described by Michaelis-Menten kinetics (Irvine et al., 1986; Togashi et al., 1997), i.e.,

$$J_{5P} = \hat{J}_{5P} \cdot \mathcal{H}_1\left(I, K_5\right) \tag{18}$$

$$J_{3K} = \hat{J}_{3K}(C) \cdot \mathcal{H}_1\,(I, K_3) \tag{19}$$

Since $K_{5P} > 10\,\mu\text{M}$ (Verjans et al., 1992; Sims and Allbritton, 1998), and such high IP_3 concentrations are unlikely to be physiological (Lemon et al., 2003; Kang and Othmer, 2009), the activity of IP-5P can be assumed far from saturation. Accordingly, the IP_3 degradation rate by IP-5P can be linearly approximated by (Stryer, 1999):

$$J_{5P} \approx \Omega_{5P} \cdot I \tag{20}$$

where $\Omega_{5P} = \hat{J}_{5P}/K_5$ is the maximal rate of IP-5P-mediated IP_3 degradation in the linear approximation.

IP_3 phosphorylation by $IP_3$3K is regulated in a complex fashion (Figure 2A). For resting conditions, when intracellular IP_3 and Ca^{2+} concentrations are below 0.1 μM, (Parpura and Haydon, 2000; Mishra and Bhalla, 2002; Kang and Othmer, 2009), it is very slow. On the other hand, as Ca^{2+} increases, $IP_3$3K activity is substantially stimulated by its phosphorylation by CaMKII in a Ca^{2+}/calmodulin (CaM)–dependent fashion (Communi et al., 1997). A further possibility could eventually be that $IP_3$3K is also inhibited by Ca^{2+}-dependent PKC phosphorylation (Sim et al., 1990), however, since evidence for the existence of such inhibitory pathway is contradictory (Communi et al., 1995), this possibility will not be taken into further consideration in this study.

Phosphorylation of $IP_3$3K by active CaMKII (i.e. CaMKII*) only occurs at a single threonine residue (Communi et al., 1997, 1999), so that it can be assumed that the rate of $IP_3$3K phosphorylation is $J^*_{3K}(C) \propto [\text{CaMKII}^*]$. On the other hand, activation of CaMKII is Ca^{2+}/CaM-dependent and occurs in a complex fashion because of the unique structure of this kinase, which is composed of ∼12 subunits, with three to four phosphorylation sites each (Kolodziej et al., 2000). Briefly, Ca^{2+} increases lead to the formation of a Ca^{2+}–CaM complex (CaM^+) that may induce phosphorylation of some of the sites of each CaMKII subunit. However, only when two of these sites at neighboring subunits are phosphorylated, CaMKII quickly and fully activates (Hanson et al., 1994). Despite the multiple CaM^+ binding reactions in the inactive kinase, experiments showed that KII activation by CaM^+ can be approximated by a Hill equation with unitary coefficient (De Konick and Schulman, 1998). Hence, the following kinetic reaction scheme for CaMKII phosphorylation can be assumed:

$$4\,\text{Ca}^{2+} + \text{CaM} \underset{\Omega_0}{\overset{O_0}{\rightleftharpoons}} \text{CaM}^+ \tag{21}$$

$$\text{KII} + \text{CaM}^+ \underset{\Omega_b}{\overset{O_b}{\rightleftharpoons}} \text{CaMKII} \underset{\Omega_i}{\overset{\Omega_a}{\rightleftharpoons}} \text{CaMKII}^* \tag{22}$$

Consider then first the binding reaction in 22. Assuming that the second step is very rapid with respect to the first one (Thiel et al., 1988; De Konick and Schulman, 1998), the generation of CaMKII* is in equilibrium with CaMKII consumption, i.e.,

$$[\text{CaMKII}^*] \approx \frac{\Omega_a}{\Omega_i}[\text{CaMKII}] \tag{23}$$

Then, under the hypothesis of quasi-steady state for CaMKII,

$$\frac{\mathrm{d}[\text{CaMKII}]}{\mathrm{d}t} = O_b\,[\text{KII}][\text{CaM}^+] - (\Omega_a + \Omega_b)\,[\text{CaMKII}] + \Omega_i\,[\text{CaMKII}^*] \approx 0 \tag{24}$$

Replacing [CaMKII*] from equation 23 in the latter equation provides

$$[\text{CaMKII}^*] = K_a K_b [\text{KII}][\text{CaM}^+] \tag{25}$$

where $K_a = \Omega_a/\Omega_i$ and $K_b = O_b/\Omega_b$. Defining the total kinase II concentration as $[\mathrm{KII}]_\mathrm{T} = [\mathrm{KII}] + [\mathrm{CaMKII}] + [\mathrm{CaMKII}^*]$ and assuming it constant, equation 25 can be rewritten as

$$[\mathrm{CaMKII}^*] = \frac{K_a[\mathrm{KII}]_T}{1+K_a} \cdot \mathcal{H}_1\left([\mathrm{CaM}^+], K_m\right) \tag{26}$$

with $K_m = \left(K_b\left(1+K_a\right)\right)^{-1}$.

The substrate concentration for the enzyme-catalyzed reaction 22 is provided by reaction 21 and reads (by QSSA)

$$[\mathrm{CaM}^+] = [\mathrm{CaM}] \cdot \mathcal{H}_4\left(C, K_0\right) \tag{27}$$

with $K_0 = O_0/\Omega_0$. Therefore, replacing the latter expression for $[\mathrm{CaM}^+]$ in equation 26, finally provides

$$[\mathrm{CaMKII}^*] = \frac{K_a[\mathrm{KII}]_\mathrm{T}}{1+K_a}\left(1+\frac{K_m}{[\mathrm{CaM}]}\right)^{-1} \cdot \mathcal{H}_4\left(C, \frac{K_0 K_m}{K_m+[\mathrm{CaM}]}\right) \tag{28}$$

Defining the Ca^{2+} affinity constant of $IP_3$3K as $K_D = K_0 K_m/\left(K_m + [\mathrm{CaM}]\right)$, the above calculations show that, despite its complexity, the reaction cascade underlying the activation of CaMKII can be concisely described by a Hill function of the Ca^{2+} concentration (C) so that $[\mathrm{CaMKII}^*] \propto \mathcal{H}_4\left(C, K_D\right)$. Accordingly, it is also $\hat{J}_{3K}(C) \propto \mathcal{H}_4\left(C, K_D\right)$, and equation 19 for $IP_3$3K-mediated IP_3 degradation can be rewritten as

$$J_{3K} = O_{3K} \cdot \mathcal{H}_4\left(C, K_D\right)\mathcal{H}_1\left(I, K_3\right) \tag{29}$$

where O_{3K} is the maximal rate of IP_3 degradation by $IP_3$3K.

3 Encoding of stimulation by combined IP_3 and Ca^{2+} dynamics

3.1 The *G-ChI* model for IP_3/Ca^{2+} signaling

A corollary of the biological and modeling arguments exposed in the previous section is that Ca^{2+} and IP_3 signals are, generally speaking, dynamically coupled in astrocytes. This implies that a complete model that mimics astrocytic IP_3 signaling must also include a description of CICR. An example of such models is the so-called *ChI* model originally introduced by De Pittà et al. (2009), which is constituted by three ODEs respectively for intracellular Ca^{2+} (C), the IP_3R gating variable h and the mass-balance equation for intracellular IP_3 lumping terms, (16), (20) and (29), i.e.

$$\frac{\mathrm{d}C}{\mathrm{d}t} = J_r(C,h,I) + J_l(C) - J_p(C) \tag{30}$$

$$\frac{\mathrm{d}h}{\mathrm{d}t} = \Omega_h(C,I)\left(h_\infty(C,I) - h\right) \tag{31}$$

$$\frac{\mathrm{d}I}{\mathrm{d}t} = O_\delta \mathcal{H}_2\left(C, K_\delta\right)\left(1-\mathcal{H}_1\left(I,\kappa_\delta\right)\right) - O_{3K}\,\mathcal{H}_4\left(C,K_D\right)\mathcal{H}_1\left(I,K_3\right) - \Omega_{5P}\,I \tag{32}$$

The above model can be extended to explicitly modeling of GPCR dynamics by a *G-ChI* model. To this aim, we add to the right-hand side of equation 32 the contribution of GPCR-mediated IP_3 synthesis given by equation 15. However, if one is interested in how GPCR kinetics evolves with IP_3 and Ca^{2+} dynamics, then the formula for J_β given by equation 2 must be used instead

of equation 15. Accordingly, the above system of equations must be completed by equation 14 for astrocytic receptor activation, i.e.

$$\frac{\mathrm{d}\Gamma_A}{\mathrm{d}t} = \dots \tag{14}$$

$$\frac{\mathrm{d}C}{\mathrm{d}t} = \dots \tag{30}$$

$$\frac{\mathrm{d}h}{\mathrm{d}t} = \dots \tag{31}$$

$$\frac{\mathrm{d}I}{\mathrm{d}t} = O_\beta \Gamma_A + O_\delta \mathcal{H}_2\left(C, K_\delta\right)\left(1 - \mathcal{H}_1\left(I, \kappa_\delta\right)\right) - O_{3K}\,\mathcal{H}_4\left(C, K_D\right)\mathcal{H}_1\left(I, K_3\right) - \Omega_{5P}\, I \tag{33}$$

Regarding the differential equations for the variables C and h above, the original formulation of the *G-ChI* model considered the Li-Rinzel description for CICR previously introduced in Chapter 3 (Li and Rinzel, 1994). In the following, we will refer to this formulation. In practice however, it must be noted that any suitable model of Ca^{2+} and IP_3R dynamics discussed in Chapters 2, 3 and 16 can be adopted in lieu of the Li-Rinzel description, and accordingly different models of *G-ChI* type may be developed, each possibly customized to study specific aspects of coupled IP_3 and Ca^{2+} signaling in astrocytes.

Figure 3 illustrates some characteristics of IP_3 and Ca^{2+} dynamics reproduced by the *G-ChI* model. In the left panel of this figure, IP_3R kinetic parameters are chosen to fit, as closely as possible, experimental data points for the steady-state open probabilities of type-2 IP_3Rs at fixed Ca^{2+} (*solid line*) and IP_3 concentrations (*dashed line*). In the right panel, the remainder of the parameters of the model are then set to reproduce (*solid black line*) a sample Ca^{2+} trace imaged by confocal microscopy on cultured astrocytes (*gray data points*). It may be observed how the associated IP_3 and h oscillations predicted by the model, are almost out of phase with respect to the Ca^{2+} ones. For h, this is due to IP_3R kinetics, whereby an increase of cytosolic Ca^{2+} promotes receptor inactivation. For IP_3 instead, this dynamics is a direct consequence of the Ca^{2+}-dependent rate of degradation of this molecule by the $IP_3$3K enzyme. This is a crucial aspect of intracellular IP_3 regulation in astrocytes which is addressed more in detail below.

3.2 Different regimes of IP_3 signaling

To develop the *G-ChI* model in Section 2, we stressed on the molecular details of the Ca^{2+} dependence of the different enzymes involved in IP_3 signaling, yet how this dependence shapes Ca^{2+} and IP_3 oscillations remains to be elucidated. With this purpose, we consider in Figure 4 the simple scenario of Ca^{2+} oscillations triggered by repetitive stimulation of an astrocyte by puffs of extracellular glutamate (*top three panels*), and look at the different contributions to IP_3 production and degradation underpinning the ensuing Ca^{2+} and IP_3 dynamics (*lower panels*). With this regard, it may be noted how the total rate of IP_3 production (*dashed line* in the *fourth panel* from top) almost resembles the dynamics of activation of astrocyte receptors (Γ_A, *second panel* from top) except for little bumps in correspondence of Ca^{2+} pulse-like elevations (*solid trace*, *third panel* from top). Consideration of the different contributions to IP_3 by PLCβ (*orange trace*) and PLCδ (*blue trace*) reveals that, while most of IP_3 production is driven by mGluR-mediated PLCβ activation, those bumps are instead caused by PLCδ, whose activation is substantially boosted during intracellular Ca^{2+} elevations.

Similar arguments also hold for IP_3 degradation (*bottom panel*). In this case, the total rate of IP_3 degradation (*dashed line*) closely mimics IP_3 dynamics in between Ca^{2+} elevations (*green trace*, *third panel* from top), and is mostly contributed by Ca^{2+}-independent IP-5P-mediated degradation (*violet trace*). This scenario however changes during Ca^{2+} elevations, when $IP_3$3K

activation becomes significant and promotes faster rates of IP_3 degradation, as mirrored by the *dashed line* which peaks in correspondence of Ca^{2+} oscillations.

Overall, these observations suggest that Ca^{2+}-independent activity of PLCβ and IP-5P vs. Ca^{2+}-dependent activation of PLCδ and $IP_3$3K account for different regimes of IP_3 signaling. One regime corresponds to low intracellular Ca^{2+} close to resting concentrations, whereby IP_3 is mainly produced by receptor-mediated activation of PLCβ against degradation by IP-5P. The other regime significantly adds to the former for sufficiently high Ca^{2+} elevations, where IP_3 production is boosted by PLCδ, but also IP_3 degradation is faster by $IP_3$3K activation.

The contribution to IP_3 production and degradation by each enzyme clearly depends on their intracellular expression as reflected by the values of the rate constants O_β, O_δ, O_{3K} and Ω_{5P} in equation 33. Nonetheless, it should be noted that the existence of different regimes of IP_3 production and degradation is regardless of these rate values, insofar as it is set by the values of the Michaelis-Menten constants of the underpinning reactions, mostly K_δ and K_D. Remarkably, estimates of these two constants are in the range of $0.1 - 1.0\,\mu M$, that is well within the range of Ca^{2+} elevations expected for an astrocyte, whose average resting Ca^{2+} concentration is reported to be $< 0.15\,\mu M$ (Zheng et al., 2015). This assures that activation of PLCδ and $IP_3$3K is effective only when intracellular Ca^{2+} approaches to, or increases beyond K_δ and K_D, as expected by the occurrence of CICR.

3.3 Signal integration

The existence of different regimes of IP_3 signaling shapes the time evolution of IP_3 with respect to stimulation in a peculiar fashion. From Figure 4 (*third panel*), it may indeed be noted that, starting from resting values, IP_3 increases for each glutamate puff almost stepwise, till it reaches a peak (or threshold) concentration (normalized to ~ 1) that triggers CICR, thereby triggering a Ca^{2+} pulse-like elevation. This Ca^{2+} elevation promotes IP_3 degradation to some concentration between its peak and baseline values, in a sort of reset mechanism, leaving IP_3 to increase back again to the CICR threshold until the next elevation. In between each Ca^{2+} elevation, counting from the first one ending at $t \approx 4\,s$, we may appreciate how IP_3 increases almost proportionally to the number of glutamate puffs, akin to an integrator of the stimulus.

This may readily be proved by analytical arguments approximating, for simplicity, each glutamate puff occurring at t_k by a Dirac's delta $\delta(t-t_k)$, so that the external stimulus impinging on the astrocyte is modeled by $Y(t) = G \cdot \Delta \sum_k \delta(t - t_k)$, where $G \cdot \Delta$ represents the glutamate concentration delivered in the time unit per puff (i.e. its dimensions are $\mu M \cdot s$). Then, assuming that in between oscillations, intracellular Ca^{2+} concentration is close to basal levels, i.e. $C \approx C_0$, with $C_0 < (\ll) K_{KC}$, K_δ, K_3 and $h \approx h_\infty$, it is possible to reduce equations 14 and 33 to

$$\frac{d\Gamma_A}{dt} \approx -(O_N Y(t) + \Omega_N)\Gamma_A + O_N Y(t) \tag{34}$$

$$\frac{dI}{dt} \approx -J_{5P} + J_\beta = -\Omega_{5P} I + O_\beta \Gamma_A \tag{35}$$

Using the fact that for puffs delivered at rate ν the identity $\int_{t'}^{t''} \sum_k \delta(t - t_k)dt = \nu(t'' - t')$ holds, we can solve equation 34 for Γ_A obtaining

$$\begin{aligned}
\Gamma_A(t) &= \int_{-\infty}^{t} O_N Y(t')\, e^{-\int_{t'}^{t}(\Omega_N + O_N Y(t''))dt''} dt' \\
&= \int_{-\infty}^{t} O_N Y(t')\, e^{-\Omega_N(t-t')}\, e^{-O_N \int_{t'}^{t} Y(t'')dt''} dt' \\
&= \int_{-\infty}^{t} O_N Y(t')\, e^{-(\Omega_N + O_N G \Delta \nu)(t-t')} dt'
\end{aligned}$$

$$= O_N Y(t') * Z_{\Gamma_A}(t) \tag{36}$$

where "$*$" denotes the convolution operator. It is thus apparent that the fraction of activated receptors $\Gamma_A(t)$ is an integral transform of the stimulus $Y(t)$ by convolution with the kernel $Z_{\Gamma_A}(t)$. Specifically, $Z_{\Gamma_A}(t)$ may be regarded as the fraction of astrocyte receptors stimulated by one extracellular glutamate puff – or equivalently, by synaptic release triggered by an action potential –, and characterizes the encoding of the stimulus by the astrocyte via its activated receptors.

The IP_3 signal resulting from the activated receptors then evolves according to

$$\begin{aligned} I(t) &= \int_{-\infty}^{t} O_\beta \Gamma_A(t')\, e^{-\int_{t'}^{t} \Omega_{5P} \mathrm{d}t''} \mathrm{d}t' = \int_{-\infty}^{t} O_\beta \Gamma_A(t')\, e^{-\Omega_{5P}(t-t')} \mathrm{d}t' \\ &= O_\beta \Gamma_A(t) * Z_I(t) \end{aligned} \tag{37}$$

That is the IP_3 signal is also an integral transform of the input stimuli through the fraction of activated receptors $\Gamma_A(t)$, by convolution with the kernel $Z_I(t) = e^{-\Omega_{5P} t}$. In particular, experimental evidence hints that the rate constant Ω_{5P} is often small compared to the rate of incoming stimulation (Appendix B), so that $Z_I(t) \approx 1$. In this case then, equation 37 predicts that $I(t) \approx \int_{-\infty}^{t} O_\beta \Gamma_A(t') \mathrm{d}t'$, namely that the IP_3 signal effectively corresponds to the integral of the fraction of activated astrocyte receptors.

It is also worth understanding the nature of the threshold concentration that IP_3 must reach in order to trigger CICR. In the *G-ChI* model, based on the Li-Rinzel description of CICR, this threshold may be not well-defined and generally varies with the parameter choice as well as with the shape and amplitude of the delivered stimulation (De Pittà et al., 2009). Consider for example Figure 5A where the Ca^{2+} response of an astrocyte (*bottom panel*) is simulated for different *color-coded* step increases of extracellular glutamate (*top panel*). It may be noted that CICR, reflected by one or multiple Ca^{2+} pulse-like increases, is triggered by glutamate concentrations greater or equal to the *orange trace*. However, the IP_3 threshold for CICR (*central panel*) appears to grow with the extracellular glutamate concentration. This is reflected by the first 'knee' of the IP_3 curves which reaches progressively higher values of IP_3 concentration as extracellular glutamate increases from *orange* to *lime* levels. At the same time, as shown by the *black dashed curve* in the *top panel* of Figure 5B, the latency for emergence of CICR since stimulus onset (*black marks* at $t = 0$) decreases. This can be explained by equations 34 and 35, noting that, while larger glutamate concentrations promote larger receptor-mediated IP_3 production, this increased production is also counteracted by faster degradation by IP-5P, since this latter linearly increases with IP_3. Thus while larger IP_3 production assures shorter delays in the onset of CICR, a larger IP_3 level must be reached to compensate for its faster degradation.

The *top panel* of Figure 5B further illustrates how the latency period for CICR onset depends on the activity of the different enzymes regulating IP_3 production and degradation. Here the different *colored curves* were obtained repeating the simulations of Figure 5A for a 50% increase of the activity respectively of PLCβ (*orange trace*), PLCδ (*blue trace*), $IP_3$3K (*red trace*) and IP-5P (*violet trace*). In agreement with our previous analysis, PLCβ and IP-5P have the largest impact on respectively reducing or increasing the latency period, given that they are the main enzymes at play in IP_3 signaling before CICR onset. The effect of an increase of IP_3 production by PLCδ is instead mainly significant for low glutamate concentrations, such that they could promote an activation of this enzyme that is comparable to that of PLCβ. Conversely, $IP_3$3K does not have any role in the control of CICR latency since its activation effectively requires CICR to onset first.

The variability of IP_3 concentrations attained to trigger CICR by different glutamate concentrations, and its correlation with the latency for CICR onset, suggest that the mere IP_3 concentration is not an effective indicator of the CICR threshold, rather we should consider instead the total IP_3 amount produced in the astrocyte cytosol during the latency period that precedes CICR onset, that is the integral in time of IP_3 concentration during such period. This is exemplified in the *bottom panel* of Figure 5B where such integral is plotted as a function of the different latency values computed in the *top panel*. It may be appreciated how this integral is essentially similar for different enzyme expressions (*colored curves*) yet associated with the same latency value.

Taken together these results put emphasis on the crucial role exerted by IP_3 signaling in the genesis of agonist-mediated Ca^{2+} elevations. In particular they suggest that the expression of different enzymes responsible of IP_3 production and degradation, which is likely heterogeneous across an astrocyte, could locally set different requirements for integration and encoding of external stimuli by the same cell.

3.4 Role of cPKCs and beyond

Different mechanisms of production and degradation of IP_3 are only one example of the possible many signaling pathways that could shape the nature of Ca^{2+} signaling in astrocytes. There is also compelling evidence in vitro that shape and duration of Ca^{2+} oscillations could be controlled by astrocyte receptor phosphorylation by cPKCs (Codazzi et al., 2001). To better understand this aspect of astrocyte Ca^{2+} signaling, we relax the quasi steady-state approximation on cPKC phsophorylation and thus rewrite equation 8 as

$$\frac{\mathrm{d}\Gamma_A}{\mathrm{d}t} = O_N[\mathrm{A}]^n\ (1-\Gamma_A) - (\Omega_N + O_K P)\,\Gamma_A \tag{38}$$

where P denotes the cPKC* concentration at the receptors' site. This in turn, requires to also consider a description of cPKC* dynamics, whereby at least two additional equations in the *G-ChI* model must be included: one that takes into account P dynamics, but also a further one that describes DAG dynamics (D), which is responsible for cPKC activation by Ca^{2+}-dependent translocation of the inactive kinase to the plasma membrane (Oancea and Meyer, 1998).

By QSSA, the quantity of cPKC* is conserved during receptor phosphorylation in reaction 4. In this fashion, cPKC* production and degradation are only controlled by the pair of reactions 9 and 10. On the other hand, taking into account from Section 2.1 that production of cPKC* depends on the availability of the Ca^{2+}-bound kinase complex cPKC$'$, we may assume at first approximation that reaction 9 for Ca^{2+}-binding to the kinase is at equilibrium, i.e. $[\mathrm{cPKC}'] = [\mathrm{cPKC}]_\mathrm{T}\,\mathcal{H}_1\,(C, K_{KC})$. Accordingly, we can consider cPKC* dynamics to be driven simply by reaction 10, i.e.

$$\begin{aligned}\frac{\mathrm{d}P}{\mathrm{d}t} &= J_{KP} - J_{KD}\\ &= O_{KD}[\mathrm{cPKC}'] \cdot D - \Omega_{KD} P\\ &= O_{KD}[\mathrm{cPKC}]_\mathrm{T}\mathcal{H}_1\,(C, K_{KC}) \cdot D - \Omega_{KD} P\\ &\equiv O_{KD}\mathcal{H}_1\,(C, K_{KC}) \cdot D - \Omega_{KD} P\end{aligned} \tag{39}$$

where we re-defined $O_{KD} \leftarrow O_{KD}[\mathrm{cPKC}]_\mathrm{T}$ as the maximal rate of cPKC* production (in $\mu\mathrm{Ms}^{-1}$).

To model DAG dynamics we start instead from the consideration that PLC isoenzymes hydrolyze PIP_2 into one molecule of IP_3 and one of DAG, so that DAG production coincides with that of IP_3 (Berridge and Irvine, 1989, and see also Figure 2B). Yet, only part of this

produced DAG is used to activate cPKC, while the rest is mainly degraded by diacylglycerol kinases (DAGKs) into phosphatidic acid (Carrasco and Mérida, 2007) and, to a minor extent, by diacylglycerol lipases (DAGLs) into 2-arachidonoylglycerol (2-AG), although this latter pathway has only been linked to some types of metabotropic receptors in astrocytes (Bruner and Murphy, 1990; Giaume et al., 1991; Walter et al., 2004). Other pathways of use of DAG are also possible in principle, inasmuch as DAG is a key molecule in the cell's lipid metabolism and a basic component of membranes. Nonetheless there is evidence that DAG levels are strictly regulated within different subcellular compartments, and DAG generated by GPCR stimulation is not usually consumed for metabolic purposes (van der Bend et al., 1994; Carrasco and Mérida, 2007).

DAGK activation reflects the sequence of Ca^{2+}mediated translocation, DAG binding and activation that is also required for cPKCs, so the two reactions may be thought to be characterized by similar kinetics, yet with an important difference. Sequence analysis of DAGKα, γ – the two isoforms of DAGKs most likely involved in astrocytic GPCR signaling (Dominguez et al., 2013) – reveals in fact the existence of two EF-hand motifs characteristics of Ca^{2+}-binding and two C1 domains for DAG binding (Mérida et al., 2008). In this fashion, a Hill exponent of 2 instead of 1 as in equation 39 must be considered for the DAGK activating reaction, so that DAGK-mediated DAG degradation can be modeled by

$$J_D = O_D \mathcal{H}_2\left(C, K_{DC}\right) \mathcal{H}_2\left(D, K_{DD}\right) \tag{40}$$

Finally, to take into account other mechanisms of DAG degradation (J_A), including but not limited to DAGLs, we assume a linear degradation rate, i.e. $J_A = \Omega_D D$. This is a crude approximation insofar as DAGL, could also be activated in a Ca^{2+}-dependent fashion (Rosenberger et al., 2007). Nonetheless, the complexity of the molecular reactions likely involved in these other pathways of DAG degradation would require to consider additional equations in our model which are beyond the scope of this chapter. The reader who is interested in these further aspects, may refer to Cui et al. (2016) for a possible modeling approach. For the purposes of our analysis instead, we will consider the following equation for DAG dynamics:

$$\begin{aligned}\frac{\mathrm{d}D}{\mathrm{d}t} &= J_\beta + J_\delta - J_{KP} - J_D - J_A \\ &= O_\beta \Gamma_A + O_\delta \mathcal{H}_2\left(C, K_\delta\right)\left(1 - \mathcal{H}_1\left(I, \kappa_\delta\right)\right) + \\ &\quad - O_{KD}\mathcal{H}_1\left(C, K_{KC}\right)\cdot D - O_D \mathcal{H}_2\left(C, K_{DC}\right)\mathcal{H}_2\left(D, K_{DD}\right) - \Omega_D D\end{aligned} \tag{41}$$

Figure 6A shows a comparison of experimental Ca^{2+} and cPKC* traces with those reproduced by the *G-ChI* model including equations 39 and 41. For inherent limitations of the Li-Rinzel description of the gating kinetics of IP_3Rs, which fails to describe these receptors' open probability for large Ca^{2+} concentration (Figure 3) and predicts fast rates of receptor de-inactivation (O_2/d_2, Table D1), the *G-ChI* model cannot generate Ca^{2+} peaks as large as those experimentally observed and shown here. Nonetheless we would like to emphasize how our model qualitatively matches experimental Ca^{2+}-dependent cPKC* dynamics, accurately reproducing the phase shift between Ca^{2+} and cPKC* oscillations. This phase shift is critically controlled by the constant K_{KC} for Ca^{2+} binding to the kinase, along with the rates of cPKC* production vs. degradation, i.e. O_{KD} vs. Ω_{KD} (equation 39), and the rate of receptor phosphorylation O_K (equation 38).

Figure 6B further reveals the role of these rate constants in the control of Ca^{2+} oscillations. In this figure, we simulated the astrocyte response for a step increase of $\sim 1.5\,\mu M$ extracellular glutamate, starting from resting conditions, both in the absence of kinase-mediated receptor phosphorylation (*gray trace*) and in the presence of it, for two different O_K rate values (*black*

traces). It may be noted how receptor phosphorylation by cPKC can rescue Ca^{2+} oscillations that otherwise would vanish by saturating intracellular IP_3 concentrations ensuing from large receptor activation. This activation indeed is decreased by cPKC* according to equation 38, thereby regulating intracellular IP_3 within the range of Ca^{2+} oscillations. Nonetheless, as the rate of receptor phosphorylation increases (*dash-dotted trace*), the period of oscillations appears to slow down and oscillations even fail to emerge, if the supply of cPKC* results in a phosphorylation rate of astrocyte receptors that exceeds their agonist-mediated activation (results not shown).

These considerations can be explained considering the period of Ca^{2+} oscillations as a function of the extracellular glutamate concentration. As shown in Figure 6C, cPKC-mediated receptor phosphorylation shifts (*black curves*) the range of glutamate concentrations that trigger Ca^{2+} oscillations to higher values than those otherwise expected in the absence of it (*gray curve*). In particular, and in agreement with experimental findings (Codazzi et al., 2001), the exact value of the rate O_K for receptor phopshorylation sets the entity of this shift, accounting either for Ca^{2+} oscillations of period longer than without receptor phosphorylation, or for the requirement of larger glutamate concentrations to observe such oscillations. This is respectively reflected by the portions of the *black curves* that are within the range of extracellular glutamate concentrations of the *gray curve*), and those that instead are not. On the other hand, longer-period oscillations in the presence of receptor phosphorylation are likely to be observed as long as the rate of cPKC* activation by DAG (O_{KD}) is below some critical value. A threefold increase of this rate indeed requires glutamate concentrations beyond those needed in the absence of receptor phosphorylation to trigger oscillations, regardless of the O_K value at play (*blue curves*). In this scenario in fact, the large supply of cPKC*, resulting from the high O_{KD} value, favors phosphorylation of receptors while hindering intracellular buildup of IP_3 to trigger CICR. This in turn requires a larger recruitment of astrocyte receptors by larger agonist concentrations to evoke Ca^{2+} oscillations.

4 Conclusions

The modeling arguments introduced in this chapter overall suggest a great richness in the possible modes whereby astrocytes could translate extracellular stimuli into intracellular Ca^{2+} dynamics. These modes are brought forth by a complex network of biochemical reactions that is exquisitely nonlinearly coupled with Ca^{2+} dynamics through different second messengers, among which IP_3 and possibly DAG could play a paramount signaling role. In particular, the regulation of different regimes of IP_3 production and degradation by Ca^{2+} in parallel with the differential regulation by this latter and DAG of the activities of cPKCs and DAGKs opens to the scenario of the existence of different regimes of signal transduction that a single astrocyte could multiplex towards different intracellular targets depending on different local conditions of neuronal activity.

An interesting implication emerging from our analysis of the regulation of the period of Ca^{2+} oscillations by cPKCs and DAG-related lipid signals is the possibility that these pathways, which could be crucially linked with inflammatory responses underpinning reactive astrocytosis (Brambilla et al., 1999; Griner and Kazanietz, 2007), could be found at different operational states, akin to what suggested for proinflammatory cytokines like TNFα (Santello and Volterra, 2012). In our analysis for example, intermediate activation of cPKC activity could promote Ca^{2+} oscillations at physiological rates, while an increase of it could exacerbate fast, potentially inflammatory Ca^{2+} responses (Sofroniew and Vinters, 2010).

Similar arguments also hold for IP_3 signaling. Calcium-dependent IP_3 production by PLCδ and PLCβ (via cPKC) could modulate the rate of integration of synaptic stimuli and thus dictate

the threshold synaptic activity triggering CICR. On the other hand, the existence of different regimes of IP_3 degradation could be responsible for different cutoff frequencies of synaptic release, beyond which integration of external stimuli by the cells could cease. In particular, this cutoff frequency could be mainly set by IP-5P during low synaptic activity, possibly associated with low intracellular Ca^{2+} levels, while be dependent on $IP_3$3K in regimes of strong astrocyte Ca^{2+} activation, and thus ultimately depend on the history of activation of the astrocyte. The following chapter looks closely at some of these aspects, focusing in particular, on the role of different IP_3 degradation regimes in the genesis and shaping of Ca^{2+} oscillations.

Appendix A Arguments of chemical kinetics

A.1 The Hill equation

In biochemistry, the binding reaction of n molecules of a ligand L to a receptor macromolecule R, i.e.,

$$\mathrm{R} + n\,\mathrm{L} \underset{k_b}{\overset{k_f}{\rightleftharpoons}} \mathrm{RL}_n \tag{42}$$

can be mathematically described by the differential equation

$$\frac{\mathrm{d}[\mathrm{RL}_n]}{\mathrm{d}t} = k_f[\mathrm{R}][\mathrm{L}]^n - k_b[\mathrm{RL}_n] \tag{43}$$

where k_f, k_b denote the forward (binding) and backward (unbinding) reaction rates respectively. At equilibrium,

$$0 = k_f[\mathrm{R}][\mathrm{L}]^n - k_b[\mathrm{RL}_n] \Rightarrow [\mathrm{RL}_n] = \frac{[\mathrm{R}][\mathrm{L}]^n}{K_d} \tag{44}$$

where $K_d = k_b/k_f$ is the *dissociation constant* of the binding reaction 42. Then, the fraction of bound receptor macromolecules with respect to the total receptor macromolecules can be expressed by the Hill equation (Stryer, 1999)

$$\frac{\text{Bound}}{\text{Total}} = \frac{[\mathrm{RL}_n]}{[\mathrm{R}] + [\mathrm{RL}_n]} = \frac{\dfrac{[\mathrm{L}]^n}{K_d}}{\dfrac{[L]^n}{K_d} + 1} = \frac{[\mathrm{L}]^n}{[\mathrm{L}]^n + K_d} = \frac{[L]^n}{[L]^n + K_{0.5}^n} = \mathcal{H}_n\left([\mathrm{L}], K_{0.5}\right) \tag{45}$$

where the function $\mathcal{H}_n\left([\mathrm{L}], K_{0.5}\right)$ denotes the sigmoid (Hill) function $[\mathrm{L}]^n \,/\, \left([\mathrm{L}]^n + {\mathrm{K}_{0.5}}^n\right)$, and $K_{0.5} = \sqrt[n]{K_d}$ is the receptor *affinity* for the ligand L, and corresponds to the ligand concentration for which half of the receptor macromolecules are bound (i.e. the midpoint of the $\mathcal{H}_n\left([\mathrm{L}], K_{0.5}\right)$ curve). The sigmoid shape of $\mathcal{H}_n\left([\mathrm{L}], K_{0.5}\right)$ denotes *saturation kinetics* in the binding reaction 42, that is, for $[\mathrm{L}] \gg K_{0.5}$ almost all the receptor molecules are bound to the ligand, so that the fraction of bound receptor molecules does not essentially change for an increase of $[L]$.

The coefficient n, also known as *Hill coefficient*, quantifies the cooperativity among multiple ligand binding sites. A Hill coefficient $n > 1$ denotes *positively cooperative binding*, whereby once one ligand molecule is bound to the receptor macromolecule, the affinity of the latter for other ligand molecules increases. Conversely, a value of $n < 1$ denotes *negatively cooperative binding*, namely when binding of one ligand molecule to the receptor decreases the affinity of the latter to bind further ligand molecules. Finally, a coefficient $n = 1$ denotes completely *independent binding* when the affinity of the receptor to ligand molecules is not affected by its state of occupation by the latter.

For unimolecular reactions, $n = 1$ coincides with the number of binding sites of the receptor. For multimolecular reactions involving $\eta > 1$ ligand molecules instead, the Hill coefficient in general, only loosely estimates the number of binding sites, being $n \leq \eta$ (Weiss, 1997). This follows from the hypothesis of total allostery that is implicit in the reaction 42, whereby the Hill function is a very simplistic way to model cooperativity. It describes in fact the limit case where affinity is 0 if no ligand is bound, and infinite as soon as one receptor binds. That is, only two states are possible: free receptor and receptor with all ligand bound. More realistic descriptions are available in literature, such as for example the Monod–Wyman–Changeux (MWC) model, but they yield much more complex equations and more parameters (Changeux and Edelstein, 2005).

A.2 The Michaelis-Menten model of enzyme kinetics

The Michaelis-Menten model of enzyme kinetics is one of the simplest and best-known models to describe the kinetics of enzyme-catalyzed chemical reactions. In general enzyme-catalyzed reactions involve an initial binding reaction of an enzyme E to a substrate S to form a complex ES. The latter is then converted into a product P and the free enzyme by a further reaction that is mediated by the enzyme itself and can be quite complex and involve several intermediate reactions. However, there is typically one rate-determining enzymatic step that allows this reaction to be modeled as a single catalytic step with an apparent rate constant k_{cat}. The resulting kinetic scheme thus reads

$$\mathrm{E} + \mathrm{S} \underset{k_b}{\overset{k_f}{\rightleftharpoons}} \mathrm{ES} \xrightarrow{k_{\text{cat}}} \mathrm{P} + \mathrm{E} \tag{46}$$

By law of mass action, the above kinetic scheme gives rise to 4 differential equations (Stryer, 1999):

$$\frac{\mathrm{d}[\mathrm{S}]}{\mathrm{d}t} = -k_f[\mathrm{E}][\mathrm{S}] + k_b[\mathrm{ES}] \tag{47a}$$

$$\frac{\mathrm{d}[\mathrm{E}]}{\mathrm{d}t} = -k_f[\mathrm{E}][\mathrm{S}] + k_b[\mathrm{ES}] + k_{\text{cat}}[\mathrm{ES}] \tag{47b}$$

$$\frac{\mathrm{d}[\mathrm{ES}]}{\mathrm{d}t} = k_f[\mathrm{E}][\mathrm{S}] - k_b[\mathrm{ES}] - k_{\text{cat}}[\mathrm{ES}] \tag{47c}$$

$$\frac{\mathrm{d}[\mathrm{P}]}{\mathrm{d}t} = k_{\text{cat}}[\mathrm{ES}] \tag{47d}$$

In the Michaelis-Menten model the enzyme is a catalyst, namely it only facilitates the reaction whereby S is transformed into P, hence its total concentration $[\mathrm{E}]_{\mathrm{T}}=[\mathrm{E}] + [\mathrm{ES}]$ must be preserved. This is indeed apparent by the sum of the second and the third equations above, since: $\frac{\mathrm{d}([\mathrm{E}]+[\mathrm{ES}])}{\mathrm{d}t} = \frac{\mathrm{d}[\mathrm{E}]_{\mathrm{T}}}{\mathrm{d}t} = 0 \Rightarrow [\mathrm{E}]_{\mathrm{T}} = \text{const}$.

The system of equations 47 can be solved for the products P as a function of the concentration of the substrate [S]. A first solution assumes instantaneous chemical equilibrium between the substrate S and the complex ES, i.e. $\frac{\mathrm{d}[\mathrm{S}]}{\mathrm{d}t} = 0$, whereby the initial binding reaction can be equivalently described by a Hill equation (Keener and Sneyd, 2008), i.e.,

$$\frac{[\mathrm{ES}]}{[\mathrm{E}]_{\mathrm{T}}} = \frac{[\mathrm{S}]}{[\mathrm{S}] + K_d} \Rightarrow [\mathrm{ES}] = \frac{[\mathrm{E}]_{\mathrm{T}}\,[\mathrm{S}]}{[\mathrm{S}] + K_d} \tag{48}$$

Alternatively, the *quasi-steady-state assumption* (QSSA) that [ES] does not change on the time scale of product formation can be made, so that $\frac{d}{dt}[\mathrm{ES}] = 0 \Rightarrow k_f[\mathrm{E}][\mathrm{S}] = k_b[\mathrm{ES}] + k_{\text{cat}}[\mathrm{ES}]$ (Keener and Sneyd, 2008), and

$$\begin{aligned} k_f[\mathrm{E}][\mathrm{S}] = k_b[\mathrm{ES}] + k_{\text{cat}}[\mathrm{ES}] &\Rightarrow k_f\left([\mathrm{E}]_{\mathrm{T}} - [\mathrm{ES}]\right)[\mathrm{S}] = k_b[\mathrm{ES}] + k_{\text{cat}}[\mathrm{ES}] \\ &\Rightarrow k_f[\mathrm{E}]_{\mathrm{T}}\,[\mathrm{S}] = \left(k_f[\mathrm{ES}][\mathrm{S}] + k_b[\mathrm{ES}] + k_{\text{cat}}[\mathrm{ES}]\right) \\ &\Rightarrow [\mathrm{ES}] = [\mathrm{E}]_{\mathrm{T}}\frac{[\mathrm{S}]}{[\mathrm{S}] + K_{\mathrm{M}}} \end{aligned} \tag{49}$$

where $K_{\mathrm{M}} = \left(k_b + k_{\text{cat}}\right)/k_f$ is the *Michaelis-Menten constant* of the reaction which quantifies the affinity of the enzyme to bind to the substrate.

Regardless of the hypothesis made to find an expression for [ES], the rate v_P of production of P can be always written as

$$v_P = \frac{\mathrm{d}[\mathrm{P}]}{\mathrm{d}t} = k_{\text{cat}}[\mathrm{ES}] = k_{\text{cat}}[\mathrm{E}]_{\mathrm{T}}\frac{[\mathrm{S}]}{[\mathrm{S}] + K_{0.5}} = v_{max}\frac{[\mathrm{S}]}{[\mathrm{S}] + K_{0.5}} \tag{50}$$

where $v_{max} = k_{\text{cat}}[\text{E}]_\text{T}$ is the maximal rate of production of P in the presence of enzyme saturation, when all the available enzyme takes part in the reaction; and the affinity constant $K_{0.5}$ equals the dissociation constant K_d of the initial binding reaction in the chemical equilibrium approximation (equation 48), or the Michaelis-Menten constant in the QSSA (equation 49).

An important corollary of the Michaelis-Menten model of enzyme kinetics is that the fraction of the total enzyme that forms the intermediate complex ES can be expressed by a Hill equation of the type

$$\frac{[\text{ES}]}{[\text{E}]_\text{T}} = \frac{[\text{S}]}{[\text{S}] + K_{0.5}} = \mathcal{H}_1\left([S], K_{0.5}\right) \tag{51}$$

and $K_{0.5}$ can be regarded as the half-saturating substrate concentration of the reaction. Similarly, the effective reaction rate v_P (equation 51) is proportional to the maximal reaction rate by a Hill-like term $\mathcal{H}_1\left([S], K_{0.5}\right)$.

Appendix B Parameter estimation

B.1 Metabotropic receptors

Rate constants O_N, Ω_N (equation 14) lump information on astrocytic metabotropic receptors' activation and inactivation, namely how long it takes for these receptors, once bound by the agonist, to trigger PLCβ-mediated IP_3 production and how long this latter lasts. Since IP_3 production mediated by agonist binding with the receptors controls the initial intracellular Ca^{2+} surge, these two rate constants may be estimated by rise times of agonist-triggered Ca^{2+} signals. With this regard, experiments reported that application of 50 µM DHPG – a potent agonist of mGluR5 which are the main type of metabotropic glutamate receptors expressed by astrocytes (Aronica et al., 2003) –, triggers submembrane Ca^{2+} signals characterized by a rise time $\tau_r = 0.272 \pm 0.095$ s. Because mGluR5 affinity ($K_{0.5}$) for DHPG is ~ 2 µM (Brabet et al., 1995), that is much smaller than the applied agonist concentration, receptor saturation may be assumed in those experiments whereby the receptor activation rate by DHPG (O_DHPG) can be expressed as a function of τ_r (Barbour, 2001), i.e. $O_\text{DHPG} \approx \tau_r/(50\,\mu\text{M}) = 0.055 - 0.113\,\mu\text{M}^{-1}\text{s}^{-1}$, so that $\Omega_\text{DHPG} = O_\text{DHPG} K_{0.5} \approx 0.11 - 0.22\,\text{s}^{-1}$. Corresponding rate constants for glutamate may then be estimated assuming similar kinetics, yet with $K_{0.5} = K_N = \Omega_N/O_N \approx 3 - 10$ µM (Daggett et al., 1995), that is 1.5–5-fold larger than $K_{0.5}$ for DHPG. Moreover, since rise times of Ca^{2+} signals triggered by non-saturating physiological stimulation are faster than in the case of DHPG (Panatier et al., 2011), it may be assumed that $O_N > O_\text{DHPG}$. With this regard, for a choice of $O_N \approx 3 \times O_\text{DHPG} = 0.3\,\mu\text{M}^{-1}\text{s}^{-1}$, with $K_N = 6$ µM such that $\Omega_N = (0.3\,\mu\text{M}^{-1}\text{s}^{-1})(6\,\mu\text{M}) = 1.8\,\text{s}^{-1}$, a peak of extracellular glutamate concentration of 250 µM, delivered at $t = 0$ and exponentially decaying at rate $\Omega_c = 40\,\text{s}^{-1}$ (Clements et al., 1992), is consistent with a peak fraction of bound receptors of ~ 0.75 within ~ 70 ms from stimulation (equation 14), which is in good agreement with experimental rise times.

B.2 IP_3R kinetics

We consider a steady-state receptor open probability in the form of $p_\text{open}(C, I) = \mathcal{H}_1^3(I, d_1) \cdot \cdot \mathcal{H}_1^3(C, d_5)(1 - \mathcal{H}_1\left(C, Q_2\right))^3$ with $Q_2 = d_2(I + d_1)/(I + d_3)$ (see Chapter 3) and choose parameters to fit corresponding experimental data by Ramos-Franco et al. (2000) for (i) different Ca^{2+} concentrations ($\hat{C}$ at a fixed IP_3 level of $\bar{I} = 1$ µM, i.e. $\hat{p}(\hat{C})$; and (ii) for different IP_3 concentrations ($\hat{I}$) at an intracellular Ca^{2+} concentration of $\bar{C} = 25$ nM, i.e. $\hat{p}(\hat{I})$. To reduce the problem dimensionality while retaining essential dynamical features of IP_3 gating kinetics we set $d_1 = d_3$ (Li and Rinzel, 1994). Accordingly, defining the vector parameter $\mathbf{x}_p = (d_1, d_2, d_5, O_2)$, we minimize the cost function $c_p(\mathbf{x}_p) = (p_\text{open}(\hat{C}, \bar{I}) - \hat{p}(\hat{C}))^2 + (p_\text{open}(\bar{C}, \hat{I}) - \hat{p}(\hat{I}))^2$ by the Artificial

Bee Colony (ABC) algorithm (Karaboga and Basturk, 2007) considering 2000 evolutions of a colony of 100 individuals.

Ultrastructural analysis of astrocytes *in situ* revealed that the probability of ER localization in the cytoplasmic space at the soma is between ∼40–70% (Pivneva et al., 2008). This suggests that the corresponding ratio between ER and cytoplasmic volumes (ρ_A) is comprised between ∼0.4–0.7.

To estimate the cell's total free Ca^{2+} content C_T we make the consideration that the resting Ca^{2+} concentration in the cytosol is $< 0.15\,\mu M$ (Zheng et al., 2015) and can be neglected with respect to the amount of Ca^{2+} stored in the ER (C_{ER}) (Berridge et al., 2003). Hence, with $C_{ER} \geq 10\,\mu M$ (Golovina and Blaustein, 1997) and a choice of $\rho_A \geq 0.4$, it follows that $C_T \approx \rho_A C_{ER} \geq 4\,\mu M$. In conditions close to store depletion during oscillations (Camello et al., 2002), this latter value would also coincide with the peak Ca^{2+} reached in the cytoplasm, which is reported between $< 5\,\mu M$ and $\sim 20\,\mu M$ (Csordàs et al., 1999; Parpura and Haydon, 2000; Kang and Othmer, 2009; Shigetomi et al., 2010).

In our simulations we set $\rho_A = 0.5$ while leaving arbitrary the choice of C_T as far as the resulting Ca^{2+} oscillations qualitatively resemble the shape of those observed in experiments. The remaining parameters for CICR, i.e. $\mathbf{z}_c = (\Omega_C, O_P)$, were chosen to approximate the number and period of Ca^{2+} oscillations observed *on average* in experiments on cultured astrocytes that were stimulated by glutamate perfusion. By "on average" we mean that we considered the average trace resulting from $n = 5$ different Ca^{2+} signals generated within the same period of time and by the same stimulus in identical experimental conditions.

B.3 IP_3 signaling

Once set the CICR parameters, individual Ca^{2+} traces used to obtained the above-mentioned "average trace" were used to search for $\mathbf{z}_p = (O_\beta, O_\delta, O_{3K}, \Omega_{5P})$, assuming random initial conditions. The ensuing parameter values were also used in Figures 4–6 although O_β, O_δ and O_{3K} were increased, from case to case, by a factor comprised between $1.2 - 2$ either to expand the oscillatory range or to promote CICR emergence (by increasing O_β, O_δ) or termination (by larger O_{3K} values).

B.4 cPKC and DAG signaling

Calcium-dependent cPKC-mediated phosphorylation has been documented for astrocytic mGluRs and P_2Y_1Rs (Codazzi et al., 2001; Hardy et al., 2005) and results in a reduction of receptor binding affinity by a factor $\zeta \approx 2 - 10$ (Hardy et al., 2005), or possibly higher depending on the cell's expression of cPKCs (Nakahara et al., 1997; Shinohara et al., 2011). Since experiments showed that cPKC is robustly activated only when Ca^{2+} increases beyond half of the peak concentration reached during oscillations (Codazzi et al., 2001) then, considering peak Ca^{2+} values of $\sim 1 - 3\,\mu M$ (Shigetomi et al., 2010) allows estimating Ca^{2+} affinity of cPKC in the range of $K_{KC} \leq 0.5 - 1.5\,\mu M$ which indeed comprises the value of $\sim 700\,nM$ predicted experimentally (Mosior and Epand, 1994). Of the same order of magnitude also is the Ca^{2+} affinity reported for DAGK, i.e. $K_{DC} \approx 0.3 - 0.4\,\mu M$ (Sakane et al., 1991; Yamada et al., 1997).

Reported values of DAG affinities for cPKC and DAGK may considerably differ. Micellar assays of cPKCs activity, suggests values of K_{KD} as low as 4.6–13.3 nM (Ananthanarayanan et al., 2003), whereas studies on purified DAGK suggest a substrate affinity for this kinase of $K_{DD} \approx 60\,\mu M$ (Kanoh et al., 1983). The differences in experimental setups and the possibility that the activity of these kinases could be widely regulated by different DAG pools make these estimate of scarce utility for our model, where the DAG concentration is of the same order of magnitude of IP_3 one. With this regard we choose to set these affinities to $0.1\,\mu M$ which

corresponded in our simulations to the average intracellular DAG concentration during Ca^{2+} oscillations.

The remaining parameters, namely $\mathbf{z}_k = (O_{KD}, O_K, \Omega_D, O_D, \Omega_D)$ were arbitrarily chosen considering two constrains: (i) DAG concentration for damped Ca^{2+} oscillations must stabilize to a constant value; and (ii) the down phase of cPKC* oscillations must follow that of Ca^{2+} ones as suggested by experimental observations by Codazzi et al. (2001).

Appendix C Software

The Python file `figures.py` used to generate the figures of this chapter can be downloaded from the online book repository at `https://github.com/mdepitta/comp-glia-book`. The software for this chapter is organized in two folders. The `data` folder contains data to fit the *G-ChI* model. WebPlotDigitizer 4.0 (`https://automeris.io/WebPlotDigitizer`) was used to extract experimental data by Ramos-Franco et al. (2000, Figures 6 and 7) and Codazzi et al. (2001, Figure 5). The Jupyter notebook file `data_loader.ipynb` found in this folder contains the code to load and clean experimental data used in the simulations.

The `code` folder contains instead all the routines (including `figures.py`) used for the simulations of this chapter. The two files `astrocyte_models.h` and `astrocyte_models.cpp` contains the core *G-ChI* model implementation in C/C++11, while the class `Astrocyte` in `astrocyte_models.py` provides the Python interface to simulate the *G-ChI* model. The model was integrated by a variable-coefficient linear multistep Adams method in Nordsieck form which proved robust to correctly solve stiff problems rising from different parameter choices (Skeel, 1986). Model fitting is provided by `gchi_fit.py` and relies on the PyGMO 2.6 optimization package (`https://github.com/esa/pagmo2.git`).

The library `gchi_bifurcation.py` provides routines to estimate the period and range of Ca^{2+} oscillation as in Figures 6. These routines use numerical continuation of the extended *G-ChI* model by the Python module PyDSTool 0.92 (Clewley, 2012, `https://github.com/robclewley/pydstool`).

Appendix D Model parameters used in simulations

Table D1. Model parameters used in the simulations, unless differently specified in figure captions.

Symbol	Description	Value	Units
	Astrocyte receptors		
Ω_N	Rate of receptor de-activation	1.8	s^{-1}
O_N	Rate of agonist-mediated receptor activation	0.3	$\mu M^{-1}s^{-1}$
n	Agonist binding cooperativity	1	–
	IP_3R kinetics		
d_1	IP_3 binding affinity	0.1	μM
O_2	Inactivating Ca^{2+} binding rate	0.325	$\mu M^{-1}s^{-1}$
d_2	Inactivating Ca^{2+} binding affinity	4.5	μM
d_3	IP_3 binding affinity (with Ca^{2+} inactivation)	0.1	μM
d_5	Activating Ca^{2+} binding affinity	0.05	μM
	Ca^{2+} fluxes		
C_T	Total ER Ca^{2+} content	5	μM
ρ_A	ER-to-cytoplasm volume ratio	0.5	–
Ω_C	Maximal Ca^{2+} release rate by IP_3Rs	7.759	s^{-1}
Ω_L	Ca^{2+} leak rate	0.1	s^{-1}
O_P	Maximal Ca^{2+} uptake rate	5.499	$\mu M s^{-1}$
K_P	Ca^{2+} affinity of SERCA pumps	0.1	μM
	IP_3 production		
O_β	Maximal rate of IP_3 production by PLCβ	0.8	$\mu M s^{-1}$
O_δ	Maximal rate of IP_3 production by PLCδ	0.025	$\mu M s^{-1}$
K_δ	Ca^{2+} affinity of PLCδ	0.5	μM
κ_δ	Inhibiting IP_3 affinity of PLCδ	1.0	μM
	IP_3 degradation		
Ω_{5P}	Rate of IP_3 degradation by IP-5P	0.86	s^{-1}
O_{3K}	Maximal rate of IP_3 degradation by $IP_3$3K	0.86	$\mu M s^{-1}$
K_D	Ca^{2+} affinity of $IP_3$3K	0.5	μM
K_{3K}	IP_3 affinity of $IP_3$3K	1.0	μM
	DAG dynamics		
Ω_D	Unspecific rate of degradation	0.26	s^{-1}
O_D	Rate of degradation by DAGK	0.45	$\mu M s^{-1}$
K_{DC}	DAGK affinity for Ca^{2+}	0.3	μM
K_{DD}	DAGK affinity for DAG	0.1	μM
	cPKC signaling		
O_{KD}	Rate of cPKC* production	0.28	$\mu M s^{-1}$
Ω_{KD}	Rate of cPKC* deactivation	0.33	s^{-1}
K_{KC}	Ca^{2+} affinity of PKC	0.5	μM
O_K	Rate of receptor phosphorylation	1.0	$\mu M^{-1}s^{-1}$

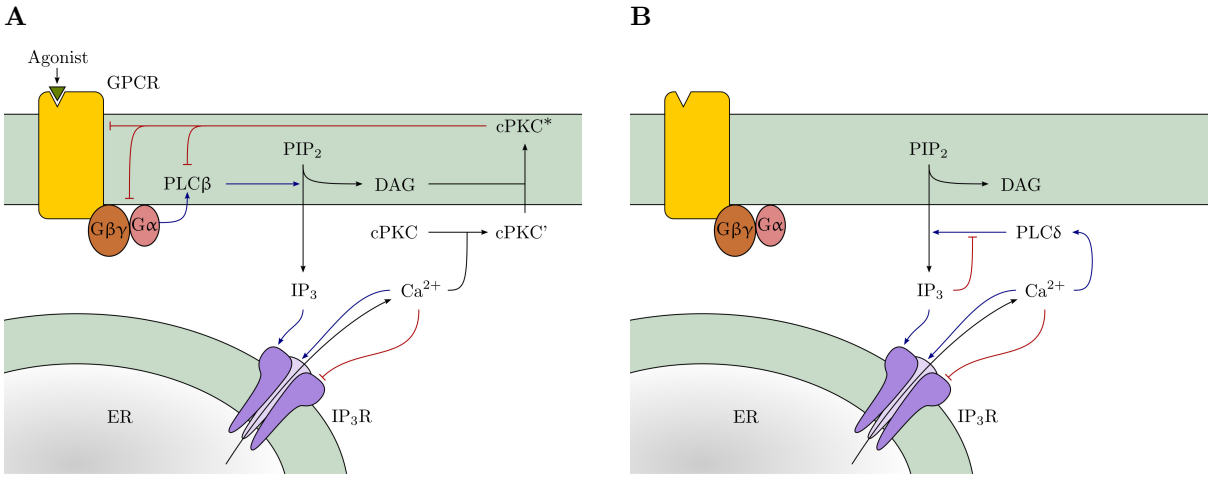

Figure 1. IP_3 production. **A** Hydrolysis of the membrane lipid phosphatidylinositol 4,5-bisphosphate (PIP_2) by PLCβ and PLCδ isoenzymes produces IP_3 and diacylglycerol (DAG). The contribution of PLCβ to IP_3 production depends on agonist binding to astrocyte G protein-coupled receptors (GPCRs). This production pathway is inhibited via receptor phosphorylation by Ca^{2+}-dependent activation of conventional protein kinases C (cPKCs). Blue: promoting pathway; *red*: inhibitory pathway.

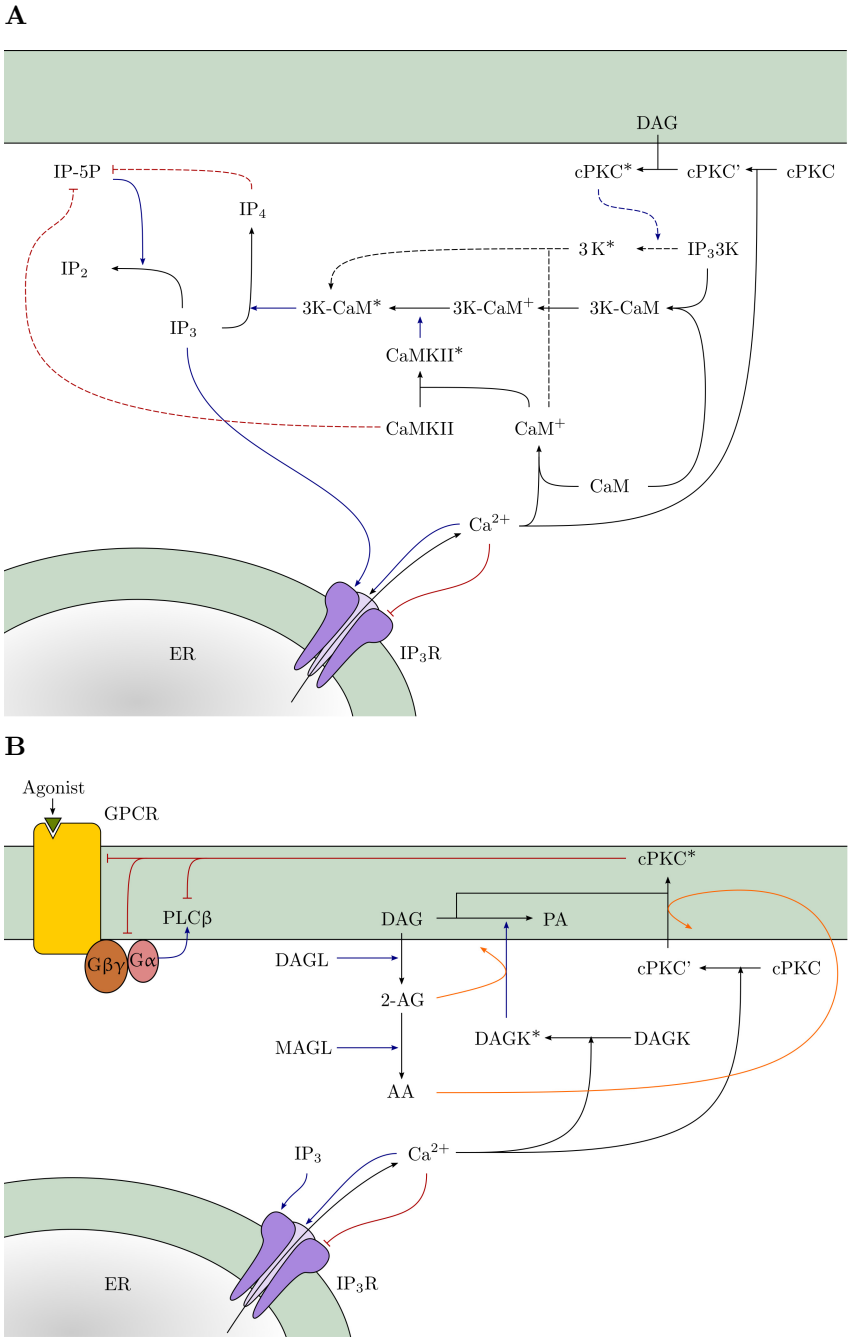

Figure 2. IP_3 and DAG degradation. **A** Degradation of IP_3 occurs by phosphorylation into inositol 1,3,4,5-tetrakisphosphate (IP_4) by $IP_3$3K and dephosphorylation into lower inositol phosphates by IP-5P. Both pathways are regulated by Ca^{2+}: $IP_3$3K activity is stimulated by phosphorylation by Ca^{2+}/calmodulin-dependent protein kinase II (CaMKII), whereas IP-5P is inhibited thereby. Moreover $IP_3$3K-mediated degradation could also be promoted by Ca^{2+} and DAG-dependent cPKC-mediated phosphorylation, while IP-5P could also be inhibited by IP_4. For the sake of simplicity, IP-5P dependence on Ca^{2+} and IP_4 along with $IP_3$3K dependence on cPKC are not taken into consideration in this study (*dashed pathways*). **B** DAG is mainly degraded into phosphatidic acid (PA) by DAG kinases (DAGK) in a Ca^{2+}-dependent fashion, and to a minor extent, into 2-arachidonoylglycerol (2-AG) by DAG lipases (DAGL). In turn 2-AG is hydrolized by monoacylglycerol lipase (MAGL) into arachidonic acid (AA). 2-AG and AA may promote activity of DAGK and cPKC* (*orange patwhays*) although this scenario is not taken into consideration here. Colors of other pathways as in Figure 1.

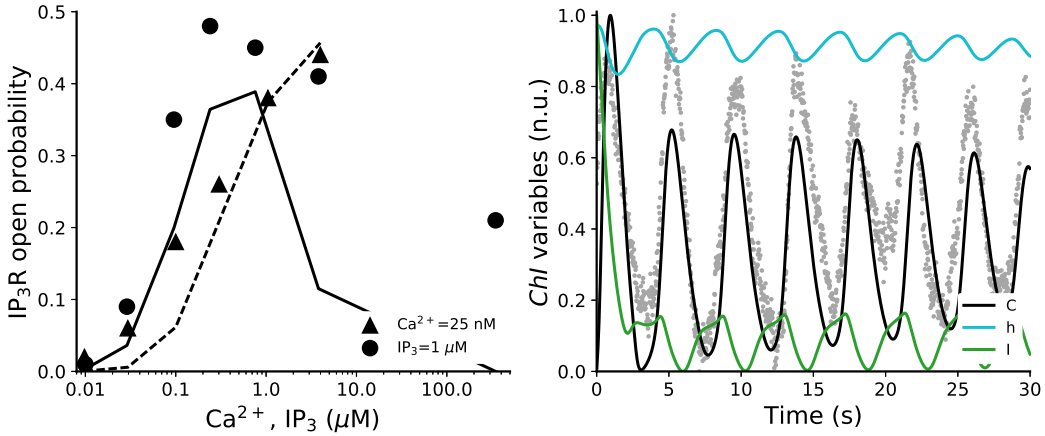

Figure 3. *G-ChI* **model**. (*left panel*) Fit of IP_3Rs kinetic parameters on experimental data of steady-state open probabilities of type-2 IP_3Rs by Ramos-Franco et al. (2000). In this example, and through all this chapter, we consider the Li-Rinzel description for CICR. This choice allows a reasonable fit (*solid and dashed lines*) of the receptors' open probability as function of either intracellular IP_3 (▲) or intracellular Ca^{2+} (●). The only exception is for Ca^{2+} concentrations $> 1\,\mu M$ for which the open probability predicted by the Li-Rinzel model (*solid line*) vanishes much more quickly than experimental values. (*right panel*) Sample Ca^{2+} (C), IP_3 (I) and h traces ensuing from a simulation of the *G-ChI* model to reproduce experimental Ca^{2+} oscillations in cultured astrocytes (*gray data points*) triggered by application of $> 5\,\mu M$ glutamate. Experimental data courtesy of Nitzan Herzog (University of Nottingham). A saturating glutamate concentration (i.e. $\Gamma_A = 1$) was assumed with initial conditions $C(0) = 0.098\,\mu M$, $h(0) = 0.972$ and $I(0) = 0.190\,\mu M$. Simulated Ca^{2+} and IP_3 traces are reported in normalized units with respect to minimum values of $C_0 = 0.1\,\mu M$ and $I_0 = 0.16\,\mu M$ and peak values of $\hat{C} = 1.42\,\mu M$ and $\hat{I} = 0.19\,\mu M$. Model parameters as in Table D1 except for $O_\beta = 0.141\,\mu M s^{-1}$ and $O_{3K} = 0.163\,\mu M s^{-1}$.

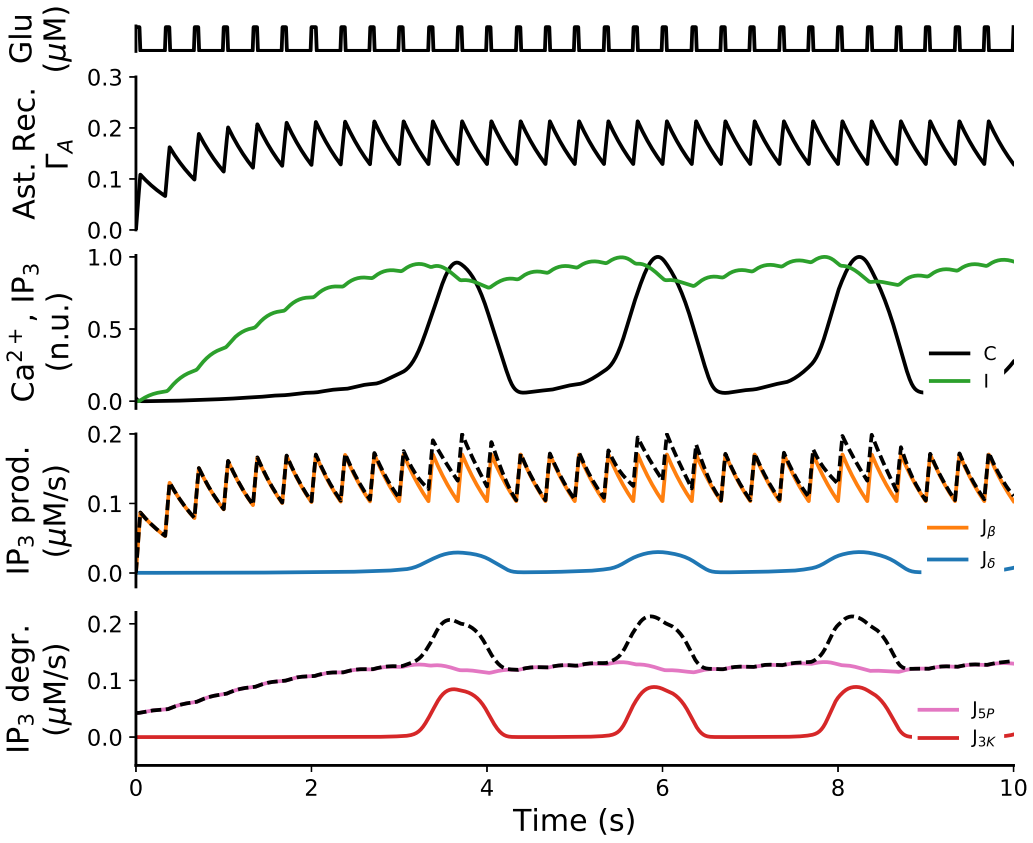

Figure 4. Coexistence of different regimes of IP_3 signaling. From top to bottom: (*first panel*) Repetitive stimulation of an astrocyte by puffs of glutamate (8 µM, rectangular pulses at rate 0.33 Hz and 15% duty cycle); (*second panel*) fraction of activated astrocytic receptors; (*third panel*) ensuing Ca^{2+} (C) and IP_3 (I) traces (normalized with respect to their maximum excursion: $C_0 = 40\,\text{nM}$, $I_0 = 50\,\text{nM}$, $\hat{C} = 0.73\,\mu\text{M}$, $\hat{I} = 0.15\,\mu\text{M}$); (*fourth panel*) total rate of IP_3 production (*dashed line*) and contributions to it by PLCβ (J_β) and PLCδ (J_δ); (*bottom panel*) total rate of IP_3 degradation (*dashed line*) resulting from the combination of degradation by IP-5P (J_{5P}) and $IP_3$3K (J_{3K}). Besides Ca^{2+} pulsed-oscillations, IP_3 is mainly regulated by PLCβ (*orange trace*) and IP-5P (*violet trace*), and its concentration tends to increase in an integrative fashion with the number of glutamate puffs. During Ca^{2+} elevations instead, activity of PLCδ (*blue trace*) and $IP_3$3K (*red trace*) become significant, with this latter responsible for a sharp drop of intracellular IP_3. Model parameters as in Table D1 except for $C_T = 10\,\mu\text{M}$, $O_P = 10\,\mu\text{Ms}^{-1}$ and $O_\delta = 0.05\,\mu\text{Ms}^{-1}$.

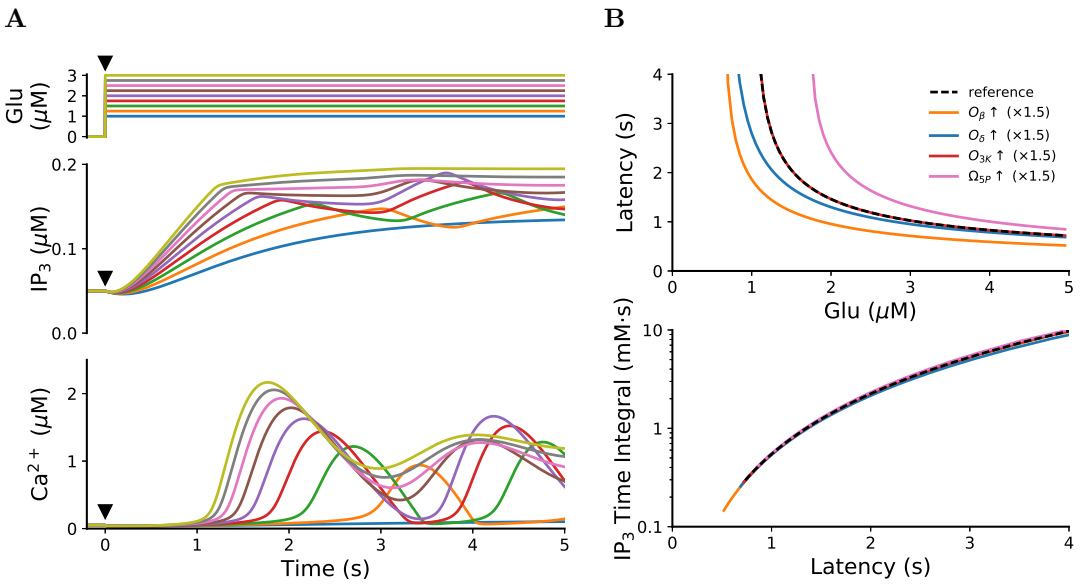

Figure 5. Threshold for CICR. **A** (*top panel*) Step increases of extracellular glutamate (*color coded*) and resulting IP_3 (*central panel*) and Ca^{2+} dynamics (*bottom panel*) in a *G-ChI* astrocyte model. *Black marks* at $t = 0$ denote stimulus onset. **B** (*top panel*) Latency for the onset of CICR as a function of the applied glutamate concentration for the Ca^{2+} traces in **A** (*black dashed curve*), as well as for 50% increases in the rate of PLCβ (O_β), PLCδ (O_δ), $IP_3$3K (O_{3K}) and IP-5P (Ω_{5P}) respectively. Emergence of CICR was detected for $\frac{dC}{dt} \geq 0.5\,\mu M/s$. (*bottom panel*) Integral of IP_3 concentration as a function of the latency values computed in the top panel. This integral is a better estimator of CICR threshold than the sole IP_3 concentration. Model parameters as Figure 4.

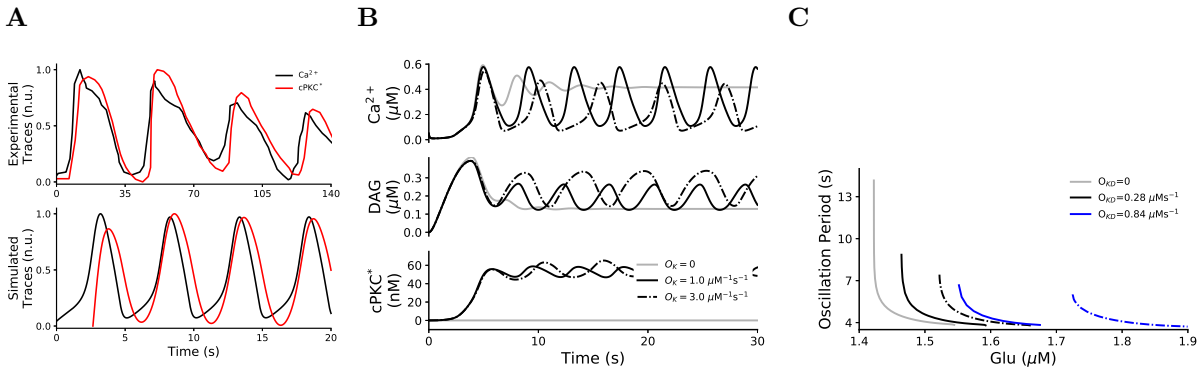

Figure 6. Regulation of Ca^{2+} oscillations by cPKC. **A** (*top panel*) Comparison between experimental traces for Ca^{2+} (*black*) and cPKC* (*red*) originally recorded in cultured astrocytes by Codazzi et al. (2001) and simulations (*bottom panel*). Despite quantitive differences in the shape and period of oscillations, the model can reproduce the essential correlation and phase shift between Ca^{2+} and cPKC* dynamics observed in experiments. Ca^{2+} and cPKC* oscillations were triggered assuming an extracellular glutamate concentration of 1.48 µM, and were normalized according to their maximum excursion: $C_0 = 0.04\,\mu M$, $P_0 = 48\,nM$, $\hat{C} = 0.49\,\mu M$ and $\hat{P} = 65\,nM$. **B** DAG and cPKC* dynamics associated with two different rates of receptor phosphorylation by cPKC (O_K, *black traces*) in response to a step increase of extracellular glutamate (1.55 µM at $t = 0$). In the absence of receptor phosphorylation (*gray traces*), Ca^{2+} oscillations would vanish due to saturating intracellular IP_3 levels ensued from large receptor activation. **C** Period of Ca^{2+} oscillations as a function of extracellular glutamate concentration. Receptor phosphorylation by cPKC critically controls the oscillatory range (*black* and *blue curves*) with respect to the scenario without cPKC activation (*gray curve*). Higher glutamate concentrations are required to trigger oscillations for larger rates of DAG-dependent cPKC activation (O_{KD}). Parameters as in Table D1 except for $\Omega_C = 6.207\,s^{-1}$, $\Omega_L = 0.01\,s^{-1}$, $O_\beta = 1\,\mu M s^{-1}$.

References

Allen, N. J. and Barres, B. A. (2009). Glia - more than just brain glue. *Nature*, 457:675–677.

Ananthanarayanan, B., Stahelin, R. V., Digman, M. A., and Cho, W. (2003). Activation mechanisms of conventional protein kinase C isoforms are determined by the ligand affinity and conformational flexibility of their C1 domains. *Journal of Biological Chemistry*, 278(47):46886–46894.

Aronica, E., Gorter, J. A., Ijlst-Keizers, H., Rozemuller, A. J., Yankaya, B., Leenstra, S., and Troost, D. (2003). Expression and functional role of mGluR3 and mGluR5 in human astrocytes and glioma cells: opposite regulation of glutamate transporter proteins. *Eur. J. Neurosci.*, 17:2106–2118.

Barbour, B. (2001). An evaluation of synapse independence. *J. Neurosci.*, 21(20):7969–7984.

Bekar, L. K., He, W., and Nedergaard, M. (2008). Locus coeruleus α-adrenergic–mediated activation of cortical astrocytes in vivo. *Cerebral cortex*, 18(12):2789–2795.

Berridge, M. J., Bootman, M. D., and Roderick, H. L. (2003). Calcium signalling: dynamics, homeostasis and remodelling. *Nat. Rev. Mol. Cell. Biol.*, 4:517–529.

Berridge, M. J. and Irvine, R. F. (1989). Inositol phosphates and cell signalling. *Nature*, 341(6239):197–205.

Bindocci, E., Savtchouk, I., Liaudet, N., Becker, D., and Carriero, G.and Volterra, A. (2017). Three-dimensional Ca^{2+} imaging advances understanding of astrocyte biology. *Science*, 356:6339.

Brabet, I., Mary, S., Bockaert, J., and Pin, J. (1995). Phenylglycine derivatives discriminate between mGluR1- and mGluR5-mediated responses. *Neuropharmacology*, 34(8):895–903.

Brambilla, R., Burnstock, G., Bonazzi, A., Ceruti, S., Cattabeni, F., and Abbracchio, M. P. (1999). Cyclo-oxygenase-2 mediates P2Y receptor-induced reactive astrogliosis. *British Journal of Pharmacology*, 126(3):563–567.

Bruner, G. and Murphy, S. (1990). ATP-evoked arachidonic acid mobilization in astrocytes is via a P2Y-purinergic receptor. *Journal of Neurochemistry*, 55(5):1569–1575.

Camello, C., Lomax, R., Petersen, O. H., and Tepikin, A. V. (2002). Calcium leak from intracellular stores - the enigma of calcium signalling. *Cell Calcium*, 32(5-6):355–361.

Carmignoto, G. (2000). Reciprocal communication systems between astrocytes and neurones. *Prog. Neurobiol.*, 62:561–581.

Carrasco, S. and Mérida, I. (2007). Diacylglycerol, when simplicity becomes complex. *Trends in Biochemical Sciences*, 32(1):27–36.

Changeux, J. and Edelstein, S. J. (2005). Allosteric mechanisms of signal transduction. *Science*, 308(5727):1424–1428.

Chen, N., Sugihara, H., Sharma, J., Perea, G., Petravicz, J., Le, C., and Sur, M. (2012). Nucleus basalis enabled stimulus specific plasticity in the visual cortex is mediated by astrocytes. *Proc. Natl. Acad. Sci. USA*, 109(41):E2832E2841.

Clements, J. D., Lester, R. A. J., Tong, G., Jahr, C. E., and Westbrook, G. L. (1992). The time course of glutamate in the synaptic cleft. *Science*, 258:1498–1501.

Clewley, R. (2012). Hybrid models and biological model reduction withPyDSTool. *PLoS Computational Biology*, 8(8):e1002628.

Codazzi, F., Teruel, M. N., and Meyer, T. (2001). Control of astrocyte Ca^{2+} oscillations and waves by oscillating translocation and activation of protein kinase C. *Curr. Biol.*, 11(14):1089–1097.

Communi, D., Dewaste, V., and Erneux, C. (1999). Calcium-calmodulin-dependent protein kinase II and protein kinase C-mediated phosphorylation and activation of D-myo-inositol 1,4,5-trisphosphate 3-kinase B in astrocytes. *J. Biol. Chem.*, 274:14734–14742.

Communi, D., Gevaert, K., Demol, H., Vandekerckhove, J., and Erneux, C. (2001). A novel receptor-mediated regulation mechanism of type I inositol polyphosphate 5-phosphatase by calcium/calmodulin-dependent protein kinase II phosphorylation. *J. Biol. Chem.*, 276(42):38738–38747.

Communi, D., Vanweyenberg, V., and Erneux, C. (1995). Molecular study and regulation of D-myo-inositol 1,4,5-trisphopshate 3-kinase. *Cell. Signal.*, 7(7):643–650.

Communi, D., Vanweyenberg, V., and Erneux, C. (1997). D-*myo*-inositol 1,4,5-trisphosphate 3-kinase A is activated by receptor activation through a calcium:calmodulin-dependent protein kinase II phosphorylation mechanism. *EMBO J.*, 16(8):1943–1952.

Connolly, T., Bansal, V., Bross, T., Irvine, R., and Majerus, P. (1987). The metabolism of tris- and tetraphosphates of inositol by 5-phosphomonoesterase and 3-kinase enzymes. *J. Biol. Chem.*, 262(5):2146–2149.

Cristóvão-Ferreira, S., Navarro, G., Brugarolas, M., Pérez-Capote, K., Vaz, S. H., Fattorini, G., Conti, F., Lluis, C., Ribeiro, J. A., McCormick, P. J., Casadó, V., Franco, R., and Sebastião, A. M. (2013). A_1R–$A_{2A}R$ heteromers coupled to g_s and $g_{i/0}$ proteins modulate GABA transport into astrocytes. *Purinergic signalling*, 9(3):433–449.

Csordàs, G., Thomas, A. P., and Hajnóczky, G. (1999). Quasi-synaptic calcium signal transmission between endoplasmic reticulum and mitochondria. *EMBO J.*, 18(1):96–108.

Cui, Y., Prokin, I., Xu, H., Delord, B., Genet, S., Venance, L., and Berry, H. (2016). Endocannabinoid dynamics gate spike-timing dependent depression and potentiation. *Elife*, 5:e13185.

Daggett, L., Sacaan, A., Akong, M., Rao, S., Hess, S., Liaw, C., Urrutia, A., Jachec, C., Ellis, S., Dreessen, J., et al. (1995). Molecular and functional characterization of recombinant human metabotropic glutamate receptor subtype 5. *Neuropharmacology*, 34(8):871–886.

De Konick, P. and Schulman, H. (1998). Sensitivity of CaM kinase II to the frequency of Ca^{2+} oscillations. *Science*, 279:227–230.

De Pittà, M., Goldberg, M., Volman, V., Berry, H., and Ben-Jacob, E. (2009). Glutamate-dependent intracellular calcium and IP_3 oscillating and pulsating dynamics in astrocytes. *J. Biol. Phys.*, 35:383–411.

De Pittà, M., Volman, V., Berry, H., Parpura, V., Liaudet, N., Volterra, A., and Ben-Jacob, E. (2013). Computational quest for understanding the role of astrocyte signaling in synaptic transmission and plasticity. *Front. Comp. Neurosci.*, 6:98.

Di Castro, M., Chuquet, J., Liaudet, N., Bhaukaurally, K., Santello, M., Bouvier, D., Tiret, P., and Volterra, A. (2011). Local Ca^{2+} detection and modulation of synaptic release by astrocytes. *Nat. Neurosci.*, 14:12761284.

Ding, F., ODonnell, J., Thrane, A. S., Zeppenfeld, D., Kang, H., Xie, L., Wang, F., and Nedergaard, M. (2013). α_1-Adrenergic receptors mediate coordinated Ca^{2+} signaling of cortical astrocytes in awake, behaving mice. *Cell Calcium*, 54(6):387–394.

Doengi, M., Hirnet, D., Coulon, P., Pape, H.-C., Deitmer, J. W., and Lohr, C. (2009). GABA uptake-dependent Ca^{2+} signaling in developing olfactory bulb astrocytes. *Proceedings of the National Academy of Sciences*, 106(41):17570–17575.

Dominguez, C. L., Floyd, D. H., Xiao, A., Mullins, G. R., Kefas, B. A., Xin, W., Yacur, M. N., Abounader, R., Lee, J. K., Wilson, G. M., Harris, T. E., and Purow, B. W. (2013). Diacylglycerol kinase α is a critical signaling node and novel therapeutic target in glioblastoma and other cancers. *Cancer Discovery*, 3(7):782–797.

Dupont, G. and Erneux, C. (1997). Simulations of the effects of inositol 1,4,5-trisphosphate 3-kinase and 5-phosphatase activities on Ca^{2+} oscillations. *Cell Calcium*, 22(5):321–331.

Erneux, C., Govaerts, C., Communi, D., and Pesesse, X. (1998). The diversity and possible functions of the inositol polyphosphate 5-phosphatases. *Biochim. Biophys. Acta*, 1436(1-2):185–189.

Essen, L., Perisic, O., Cheung, R., Katan, M., and Williams, R. L. (1996). Crystal structure of a mammalian phosphoinositide-specific phospholipase C. *Nature*, 380:595–602.

Essen, L., Perisic, O., Lunch, D. E., Katan, M., and Williams, R. L. (1997). A ternary metal binding site in the C2 domain of phosphoinositide-specific phospholipase C-δ1. *Biochemistry (Mosc.)*, 37(10):4568–4680.

Fam, S., Gallagher, C., and Salter, M. (2000). $P2Y_1$ purinoceptor-mediated Ca^{2+} signaling and Ca^{2+} wave propagation in dorsal spinal cord astrocytes. *J. Neurosci.*, 20(8):2800–2808.

Fisher, S. K. (1995). Homologous and heterologous regulation of receptor-stimulated phosphoinosited hydrolysis. *Eur. J. Pharmacol.*, 288:231–250.

Gallo, V. and Ghiani, A. (2000). Glutamate receptors in glia: new cells, new inputs and new functions. *Trends Pharm. Sci.*, 21:252–258.

Giaume, C., Marin, P., Cordier, J., Glowinski, J., and Premont, J. (1991). Adrenergic regulation of intercellular communications between cultured striatal astrocytes from the mouse. *Proceedings of the National Academy of Sciences*, 88(13):5577–5581.

Golovina, V. A. and Blaustein, M. P. (1997). Spatially and functionally distinct Ca^{2+} stores in sarcoplasmic and endoplasmic reticulum. *Science*, 275:1643–1648.

Griner, E. M. and Kazanietz, M. G. (2007). Protein kinase C and other diacylglycerol effectors in cancer. *Nature Reviews Cancer*, 7(4).

Hanson, P. I., Meyer, T., Stryer, L., and Schulman, H. (1994). Dual role of calmodulin in autophosphorylation of multifunctional CaM kinase may underlie decoding of calcium signals. *Neuron*, 12:943–956.

Hardy, A., Conley, P., Luo, J., Benovic, J., Poole, A., and Mundell, S. (2005). P2Y1 and P2Y12 receptors for ADP desensitize by distinct kinase-dependent mechanisms. *Blood*, 105(9):3552–3560.

Heller, J. P. and Rusakov, D. A. (2015). Morphological plasticity of astroglia: understanding synaptic microenvironment. *Glia*, 63(12):2133–2151.

Hermosura, M., Takeuchi, H., Fleig, A., Riley, A., Potter, B., Hirata, M., and Penner, R. (2000). InsP4 facilitates store-operated calcium influx by inhibition of InsP3 5-phosphatase. *Nature*, 408(6813):735–740.

Höfer, T., Venance, L., and Giaume, C. (2002). Control and plasticity of intercellular calcium waves in astrocytes: a modeling approach. *J. Neurosci.*, 22(12):4850–4859.

Irvine, R. F., Letcher, A. J., Heslop, J. P., and Berridge, M. J. (1986). The inositol tris/tetrakisphopshate pathway–demonstration of Ins(1,4,5)P_3 3-kinase activity in animal tissues. *Nature*, 320:631–634.

Irvine, R. F. and Schell, M. J. (2001). Back in the water: the return of the inositol phosphates. *Nat. Rev. Mol. Cell Biol.*, 2(5):327–338.

Jennings, A., Tyurikova, O., Bard, L., Zheng, K., Semyanov, A., Henneberger, C., and Rusakov, D. A. (2017). Dopamine elevates and lowers astroglial Ca^{2+} through distinct pathways depending on local synaptic circuitry. *Glia*, 65(3):447–459.

Jourdain, P., Bergersen, L. H., Bhaukaurally, K., Bezzi, P., Santello, M., Domercq, M., Matute, C., Tonello, F., Gundersen, V., and Volterra, A. (2007). Glutamate exocytosis from astrocytes controls synaptic strength. *Nat. Neurosci.*, 10(3):331–339.

Kang, J., Jiang, L., Goldman, S. A., and Nedergaard, M. (1998). Astrocyte-mediated potentiation of inhibitory synaptic transmission. *Nat. Neurosci.*, 1(8):683–692.

Kang, M. and Othmer, H. (2009). Spatiotemporal characteristics of calcium dynamics in astrocytes. *Chaos*, 19(3):037116.

Kanoh, H., Kondoh, H., and Ono, T. (1983). Diacylglycerol kinase from pig brain. Purification and phospholipid dependencies. *Journal of Biological Chemistry*, 258(3):1767–1774.

Karaboga, D. and Basturk, B. (2007). A powerful and efficient algorithm for numerical function optimization: artificial bee colony (ABC) algorithm. *Journal of Global Optimization*, 39(3):459–471.

Keener, J. and Sneyd, J. (2008). *Mathematical Physiology: I: Cellular Physiology*, volume 1. Springer.

Kolodziej, S. J., Hudmon, A., Waxham, M. N., and Stoops, J. K. (2000). Three-dimensional reconstructions of calcium/calmodulin-dependent (CaM) kinase IIα and truncated CaM kinase IIα reveal a unique organization for its structural core and functional domains. *J. Biol. Chem.*, 275(19):14354–14359.

Lemon, G., Gibson, W. G., and Bennett, M. R. (2003). Metabotropic receptor activation, desensitization and sequestration – I: modelling calcium and inositol 1,4,5-trisphosphate dynamics following receptor activation. *Journal of Theoretical Biology*, 223(1):93–111.

Li, Y. and Rinzel, J. (1994). Equations for $InsP_3$ receptor-mediated $[Ca^{2+}]_i$ oscillations derived from a detailed kinetic model: A Hodgkin-Huxley like formalism. *J. Theor. Biol.*, 166:461–473.

Losi, G., Mariotti, L., and Carmignoto, G. (2014). GABAergic interneuron to astrocyte signalling: a neglected form of cell communication in the brain. *Phil. Trans. Royal Soc. B: Biological Sciences*, 369(1654):20130609.

Marinissen, M. J. and Gutkind, J. S. (2001). G-protein-coupled receptors and signaling networks: emerging paradigms. *Trends in Pharmacological Sciences*, 22(7):368–376.

Mariotti, L., Losi, G., Sessolo, M., Marcon, I., and Carmignoto, G. (2016). The inhibitory neurotransmitter GABA evokes long-lasting Ca^{2+} oscillations in cortical astrocytes. *Glia*, 64(3):363–373.

Martín, R., Bajo-Grañeras, R., Moratalla, R., Perea, G., and Araque, A. (2015). Circuit-specific signaling in astrocyte-neuron networks in basal ganglia pathways. *Science*, 349(6249):730–734.

Mérida, I., Ávila-Flores, A., and Merino, E. (2008). Diacylglycerol kinases: at the hub of cell signalling. *Biochemical Journal*, 409(1):1–18.

Min, R. and Nevian, T. (2012). Astrocyte signaling controls spike timing-dependent depression at neocortical synapses. *Nat. Neurosci.*, 15(5):746–753.

Mishra, J. and Bhalla, U. S. (2002). Simulations of inositol phosphate metabolism and its interaction with $InsP_3$-mediated calcium release. *Biophys. J.*, 83:1298–1316.

Mosior, M. and Epand, R. M. (1994). Characterization of the calcium-binding site that regulates association of protein kinase C with phospholipid bilayers. *Journal of Biological Chemistry*, 269(19):13798–13805.

Nakahara, K., Okada, M., and Nakanishi, S. (1997). The metabotropic glutamate receptor mGluR5 induces calcium oscillations in cultured astrocytes via protein kinase C phosphorylation. *J. Neurochem.*, 69(4):1467–1475.

Navarrete, M. and Araque, A. (2008). Endocannabinoids mediate neuron-astrocyte communication. *Neuron*, 57(6):883–893.

Navarrete, M., Perea, G., de Sevilla, D., Gómez-Gonzalo, M., Núñez, A., Martín, E., and Araque, A. (2012). Astrocytes mediate in vivo cholinergic-induced synaptic plasticity. *PLoS Biol.*, 10(2):e1001259.

Nishizuka, Y. (1995). Protein kinase C and lipid signaling for sustained cellular responses. *FASEB J.*, 9:484–496.

Oancea, E. and Meyer, T. (1998). Protein kinase C as a molecular machine for decoding calcium and diacylglycerol signals. *Cell*, 95:307–318.

Ochocka, A.-M. and Pawelczyk, T. (2003). Isozymes delta of phosphoinositide-specific phospholipase C and their role in signal transduction in the cell. *Acta Biochimica Polonica*, 50(4):1097–1110.

Overington, J. P., Al-Lazikani, B., and Hopkins, A. L. (2006). How many drug targets are there? *Nature Reviews Drug discovery*, 5(12):993–996.

Panatier, A., Vallée, J., Haber, M., Murai, K., Lacaille, J., and Robitaille, R. (2011). Astrocytes are endogenous regulators of basal transmission at central synapses. *Cell*, 146:785–798.

Parpura, V. and Haydon, P. G. (2000). Physiological astrocytic calcium levels stimulate glutamate release to modulate adjacent neurons. *Proc. Natl. Acad. Sci. USA*, 97(15):8629–8634.

Parri, H. R. and Crunelli, V. (2003). The role of Ca^{2+} in the generation of spontaneous astrocytic Ca^{2+} oscillations. *Neuroscience*, 120(4):979–992.

Pawelczyk, T. and Matecki, A. (1997). Structural requirements of phospholipase C $\delta 1$ for regulation by spermine, sphingosine and sphingomyelin. *Eur. J. Biochem.*, 248:459–465.

Perea, G. and Araque, A. (2005a). Synaptic regulation of the astrocyte calcium signal. *J. Neur. Transmission*, 112:127–135.

Pivneva, T., Haas, B., Reyes-Haro, D., Laube, G., Veh, R., Nolte, C., Skibo, G., and Kettenmann, H. (2008). Store-operated Ca^{2+} entry in astrocytes: different spatial arrangement of endoplasmic reticulum explains functional diversity in vitro and in situ. *Cell Calcium*, 43(6):591–601.

Ramos-Franco, J., Bare, D., Caenepeel, S., Nani, A., Fill, M., and Mignery, G. (2000). Single-channel function of recombinant type 2 inositol 1,4,5-trisphosphate receptor. *Biophys. J.*, 79(3):1388–1399.

Rebecchi, M. J. and Pentyala, S. N. (2000). Structure, function, and control of phosphoinositide-specific phospholipase C. *Physiol. Rev.*, 80(4):1291–1335.

Rhee, S. G. and Bae, Y. S. (1997). Regulation of phosphoinositide-specific phospholipase C isozymes. *J. Biol. Chem.*, 272:15045–15048.

Rosenberger, T. A., Farooqui, A. A., and Horrocks, L. A. (2007). Bovine brain diacylglycerol lipase: substrate specificity and activation by cyclicAMP-dependent protein kinase. *Lipids*, 42(3):187–195.

Ryu, S. H., Kin, U., Wahl, M. I., Brown, a. b., Carpenter, G., Huang, K., and Rhee, S. G. (1990). Feedback regulation of phospholipase C-β by protein kinase C. *J. Biol. Chem.*, 265(29):17941–17945.

Sakane, F., Yamada, K., Imai, S.-I., and Kanoh, H. (1991). Porcine 80-kDa diacylglycerol kinase is a calcium-binding and calcium/phospholipid-dependent enzyme and undergoes calcium-dependent translocation. *Journal of Biological Chemistry*, 266(11):7096–7100.

Santello, M. and Volterra, A. (2012). TNFα in synaptic function: switching gears. *Trends in Neurosci.*, 35(10):638–647.

Serrano, A., Haddjeri, N., Lacaille, J., and Robitaille, R. (2006). GABAergic network activation of glial cells underlies heterosynaptic depression. *J. Neurosci.*, 26(20):5370–5382.

Shigetomi, E., Kracun, S., Sovfroniew, M. S., and Khakh, B. S. (2010). A genetically targeted optical sensor to monitor calcium signals in astrocyte processes. *Nat. Neurosci.*, 13(6):759–766.

Shinohara, T., Michikawa, T., Enomoto, M., Goto, J., Iwai, M., Matsu-ura, T., Yamazaki, H., Miyamoto, A., Suzuki, A., and Mikoshiba, K. (2011). Mechanistic basis of bell-shaped dependence of inositol 1,4,5-trisphosphate receptor gating on cytosolic calcium. *Proc. Natl. Acad. Sci. USA*, 108(37):15486–15491.

Shinomura, T., Asaoka, Y., Oka, M., Yoshida, K., and Nishizuka, Y. (1991). Synergistic action of diacylglycerol and unsaturated fatty acid for protein kinase C activation: Its possible implications. *Proc. Natl. Acad. Sci. USA*, 88:5149–5153.

Sim, S. S., Kim, J. W., and Rhee, S. G. (1990). Regulation of D-myo-inositol 1,4,5-trisphosphate 3-kinase by cAMP-dependent protein kinase and protein kinase c. *J. Biol. Chem.*, 265:10367–10372.

Sims, C. E. and Allbritton, N. L. (1998). Metabolism of inositol 1,4,5-trisphosphate and inositol 1,3,4,5-tetrakisphosphate by the oocytes of *Xenopus laevis*. *J. Biol. Chem.*, 273(7):4052–4058.

Skeel, R. D. (1986). Construction of variable-stepsize multistep formulas. *Mathematics of Computation*, 47(176):503–510.

Sofroniew, M. V. and Vinters, H. V. (2010). Astrocytes: biology and pathology. *Acta Neuropathol.*, 119(1):7–35.

Stryer, L. (1999). *Biochemistry*. W. H. Freeman and Company, New York, 4th edition.

Suh, P.-G., Park, J.-I., Manzoli, L., Cocco, L., Peak, J. C., Katan, M., Fukami, K., Kataoka, T., Yun, S., and Ryu, S. H. (2008). Multiple roles of phosphoinositide-specific phospholipase C isozymes. *BMB Reports*, 41(6):415–34.

Sun, W., McConnell, E., Pare, J.-F., Xu, Q., Chen, M., Peng, W., Lovatt, D., Han, X., Smith, Y., and Nedergaard, M. (2013). Glutamate-dependent neuroglial calcium signaling differs between young and adult brain. *Science*, 339(6116):197–200.

Suzuki, Y., Moriyoshi, E., Tsuchiya, D., and Jingami, H. (2004). Negative cooperativity of glutamate binding in the dimeric metabotropic glutamate receptor subtype I. *J. Biol. Chem.*, 279(34):35526–35534.

Takata, N., Mishima, T., Hisatsune, C., Nagai, T., Ebisui, E., Mikoshiba, K., and Hirase, H. (2011). Astrocyte calcium signaling transforms cholinergic modulation to cortical plasticity *in vivo*. *J. Neurosci.*, 31(49):18155–18165.

Thiel, G., Czernik, A. J., Gorelick, F., Nairn, A. C., and Greengard, P. (1988). Ca^{2+}/calmodulin-dependent protein kinase II: Identification of threonine-286 as the autophosphorylation site in the α subunit associated with the generation of Ca^{2+}-independent activity. *Proc. Natl. Acad. Sci. USA*, 85:6337–6341.

Togashi, S., Takazawa, K., Endo, T., Erneux, C., and Onaya, T. (1997). Structural identification of the *myo*-inositol 1,4,5-trisphosphate-binding domain in rat brain inositol 1,4,5-trisphopshate 3-kinase. *Biochem. J.*, 326:221–225.

Vaarmann, A., Gandhi, S., and Abramov, A. Y. (2010). Dopamine induces Ca^{2+} signaling in astrocytes through reactive oxygen species generated by monoamine oxidase. *Journal of Biological Chemistry*, 285(32):25018–25023.

van der Bend, R. L., de Widt, J., Hilkmann, H., and Van Blitterswijk, W. J. (1994). Diacylglycerol kinase in receptor-stimulated cells converts its substrate in a topologically restricted manner. *Journal of Biological Chemistry*, 269(6):4098–4102.

Verjans, B., Lecocq, R., Moreau, C., and Erneux, C. (1992). Purification of bovine brain inositol-1,4,5-trisphosphate 5-phosphatase. *Eur. J. Biochem.*, 204:1083–1087.

Violin, J. D., Crombie, A. L., Soergel, D. G., and Lark, M. W. (2014). Biased ligands at G-protein-coupled receptors: promise and progress. *Trends in Pharmacological Sciences*, 35(7):308–316.

Volterra, A., Liaudet, N., and Savtchouk, I. (2014). Astrocyte Ca^{2+} signalling: an unexpected complexity. *Nature Reviews Neuroscience*, 15:327–334.

Walter, L., Dinh, T., and Stella, N. (2004). ATP induces a rapid and pronounced increase in 2-arachidonoylglycerol production by astrocytes, a response limited by monoacylglycerol lipase. *Journal of Neuroscience*, 24(37):8068–8074.

Wang, X., Lou, N., Xu, Q., Tian, G.-F., Peng, W. G., Han, X., Kang, J., Takano, T., and Nedergaard, M. (2006). Astrocytic Ca^{2+} signaling evoked by sensory stimulation *in vivo*. *Nat. Neurosci.*, 9(6):816–823.

Weiss, J. N. (1997). The Hill equation revisited: uses and misuses. *FASEB J.*, 11:835–841.

Yamada, K., Sakane, F., Matsushima, N., and Kanoh, H. (1997). EF-hand motifs of α, β and γ isoforms of diacylglycerol kinase bind calcium with different affinities and conformational changes. *Biochemical Journal*, 321(1):59–64.

Zheng, K., Bard, L., Reynolds, J. P., King, C., Jensen, T. P., Gourine, A. V., and Rusakov, D. A. (2015). Time-resolved imaging reveals heterogeneous landscapes of nanomolar Ca^{2+} in neurons and astroglia. *Neuron*, 88(2):277–288.

Zorec, R., Araque, A., Carmignoto, G., Haydon, P., Verkhratsky, A., and Parpura, V. (2012). Astroglial excitability and gliotransmission: An appraisal of Ca^{2+} as a signaling route. *ASN Neuro*, 4(2):e00080.